https://doi.org/10.1016/j.jcsr.2021.106681 

# Lean duplex stainless steel tubular sections undergoing web crippling at elevated temperatures

Yancheng Cai [a], Liping Wang [b,d*] and Feng Zhou [c]

[a] Department of Civil and Environmental Engineering, The Hong Kong Polytechnic University, Hong Kong, China
[b] School of Civil Engineering, Central South University, Changsha, 410075, China
[c] Department of Structural Engineering, Tongji University, Shanghai, China
[d] Engineering Technology Research Center for Prefabricated Construction Industrialization of Hunan Province, Changsha, 410075, China

## Abstract

Codified design rules for web crippling of stainless steel tubular sections at elevated temperatures are currently not available. In this study, non-linear finite element models (FEMs) were developed for the web crippling of cold-formed lean duplex stainless steel (CFLDSS) square and rectangular hollow sections under the concentrated interior bearing loads, namely, the loading conditions of Interior-One-Flange (IOF), Interior-Two-Flange (ITF) and Interior Loading (IL). After successful validation of the FEMs, an extensive parametric study of 210 CFLDSS tubular sections at elevated temperatures (up to 950 °C) was performed. The appropriateness of the web crippling design rules in the current international specifications and literature was examined by comparing their ultimate strength predictions with those obtained from the numerical parametric study. During the calculation, the material properties at room (ambient) temperature condition were substituted by those at elevated temperatures. It was found that the predictions by the North American Specification were generally unconservative and not reliable, while the European Code provided reliable but generally very conservative predictions. New design method is proposed, including a new equation and the modified Direct Strength Method, for the web crippling of CFLDSS tubular sections at elevated temperatures under the loading conditions of IOF, ITF and IL. The assessment indicated that the predictions by using the new method are generally conservative and reliable.

**Keywords**: Concentrated bearing loads, direct strength method, elevated temperatures, lean duplex stainless steel, finite element analysis, web crippling.

* Corresponding author.
E-mail address: wlp2016@csu.edu.cn (L. Wang).

## 1 Introduction

The excellent properties of stainless steel, such as corrosion resistance, oxidation resistance and fire resistance, make it suitable for a wide range of application in engineering structures. The alloying elements of stainless steel have been continuingly developed for the goal of better mechanical properties, and higher corrosion resistance in high temperature application [1]. The relatively new stainless steel, lean duplex stainless steel (such as EN 1.4062 and EN 1.4162), is a high strength material with nominal 0.2% proof stress of 450 MPa. It offers higher strength than the traditional stainless steel, but has superior economic advantages due to its lower nickel content (around 1.5%), as the cost mainly depends on the nickel price. Therefore, it is becoming an attractive choice as a construction material in civil and structural engineering industry, for example, it is used in the footbridge in Siena [2]. It should be noted that the lean duplex stainless steel is not covered in the current American (ASCE) [3]) and Australian/New Zealand (AS/NZS) [4] stainless steel design specifications, while it was recently introduced in the European Code (EC3-1.4) [5].

In the past few years, great progress has been made in understanding and improving the structural properties and design criteria of lean duplex stainless steel. These efforts include the fundamental material properties by the tensile coupon tests [6,7], and structural members, such as beams [7,8], columns [9-11], plate girders [12,13], and the connections by bolts [14]. In these investigations, the design rules from the stainless steel specifications of ASCE [2], AS/NZS [3] and European Code [15] were evaluated. Investigations have also been made to modify design equations or derive new design methods to better predict the strength of lean duplex stainless steel structures. However, it should be noted that these investigations were conducted at room (ambient) temperature condition instead of under elevated temperatures. Hence, effects on the structural behaviour due to elevated temperatures were considered and investigated in this paper.

Many studies have been carried out for the structural behaviour and design of carbon steel members at elevated temperatures. The structural behavior and failure modes of cold-formed lipped channels at elevated temperatures were investigated [16, 17]. Different members were also conducted by other researchers, such as the study of high strength steel columns [18], light gauge compression members [19], channel section beams [20], lipped channel beams [21], as well as SHS and RHS beams [22]. It has been recognized that stainless steel has better strength and stiffness retention than carbon steel at elevated temperatures. This superior performance has been utilized in the high temperature industry for many years [23]. In the last few years, attention has been received to investigate the structural performance and develop the design rules for stainless steel structures at elevated temperatures, for examples, the beams [24] and tubular joints [25] that fabricated by austenitic stainless steel (EN 1.4301) and duplex stainless steel (EN 1.4462), as well as bolted connections that fabricated by lean duplex stainless steel (EN 1.4162) [26-29]. However, few investigations have been conducted on lean duplex stainless steel undergoing web crippling at elevated temperatures, which is the focus of this paper.

For steel members under concentrated loads, web crippling failure is an important issue that should be carefully considered in the design. The web crippling design rules for cold-formed stainless steel structures in current specifications [3-5] are generally empirical in nature and are based on those for cold-formed carbon steel [30]. It has been found that the current design rules are generally not able to provide accurate and reliable predictions for the web crippling strengths of stainless steel members including cold-formed high-strength stainless steel square and rectangular hollow sections, ferritic stainless steel tubular members [31-32], ferritic stainless steel square and rectangular hollow sections [33], ferritic stainless steel cold formed sections [34], and stainless steel I-sections [35,36].

More recent experimental investigations of over 100 cold-formed lean duplex stainless steel (CFLDSS) tubular members undergoing web crippling carried out by Cai and Young [37,38] showed that the strengths predicted by the current stainless steel [3-5] and carbon steel [39] design specifications, as well as the design rules in the literature [40] were generally conservative. Even the design of lean duplex stainless steel members at room temperature condition has not yet been included in the existing international codes [3, 4], (except the EC3-1.4 [5]), not to mention its design at elevated temperatures. Hence, it is firstly proposed herein to investigate the structural behaviour and design of CFLDSS tubular sections undergoing web crippling by interior loading conditions at elevated temperatures. The sections were under the three interior loading conditions of Interior-One-Flange (IOF), Interior-Two-Flange (ITF) and interior loading (IL) at the nominal elevated temperatures ranged from 22 to 950 °C. The web crippling design rules at room temperature in the current aforementioned design specifications [3-5, 39] are examined for the possibility of application at elevated temperatures. In doing so, the reduced material properties due to elevated temperatures are used in calculating the web crippling strengths. The design rules in literature was also assessed. Finally, new design method, including a new equation and the modified Direct Design Method (DSM) is proposed for the design of CFLDSS tubular sections subjected to web crippling at elevated temperatures.

## 2 Summary of test program

The tests carried out by Cai and Young [38] for CFLDSS tubular sections subjected to web crippling failure under concentrated interior bearing loads (IOF, ITF and IL) were under room (ambient) temperature condition. The test strengths and failure modes of the sections were provided by the test results. It should be mentioned that the loading conditions of IOF and ITF referred to those stated in the existing stainless steel design specifications, such as ASCE [3] and AS/NZS [4]; while the IL loading condition simulated the floor joist members placed on a solid foundation under concentrated interior bearing load.

The CFLDSS had square and rectangular hollow sections ($H$×$B$×$t$) with grades of EN 1.4162 (AISI S32101) and EN 1.4062 (AISI S32202). The definition of the symbols in a CFLDSS section are shown in Figure 1, where $H$ and $h$ are respectively the over height and the flat portion of the section web; $B$ and $t$ are the respective width and thickness of the section. The CFLDSS were used to fabricate the test specimens. The tensile flat coupon tests were carried out to obtain the material properties of the CFLDSS at room temperature condition. The material properties, including the Young's modulus ($E_r$), 0.2% proof stress ($f_{0.2,r}$) and ultimate strength ($f_{u,r}$) at room temperature were obtained from the tensile flat coupons and summarized in Table 1. Detailed description of the coupon tests are given in Cai and Young [37].

The numerical verifications for the test specimens and test strengths ($P_t$) of CFLDSS specimens are shown in Table 2. These specimens were tested under the loading conditions of IOF, ITF and IL. The specimens were generally identified by three segments in the labelling. For example of Specimen IOF100×100×3.0N90, where the first segment "IOF" indicates the loading condition of "Interior-One-Flange"; the following segment of "100×100×3.0" means the section dimension of "$H$×$B$×$t$" in the unit of mm; and the last segment "N90" indicates that the loading plate with bearing length ($N$) of $N$ = 60 mm was used in the test specimen. To identify a repeated specimen, an additional segment of "-r" was used at the end of the labelling, e.g., repeated specimen of IOF100×100×3.0N90-r. It should be noted that the flanges of the CFLDSS specimens [38] were not fastened to the steel loading plates in the test program. The hydraulic actuator was driven with a constant loading rate of 0.3 mm/min for all test specimens using the displacement control test method. Detailed description of the test setups and testing procedures were given in Cai and Young [38].

# 3 Finite element models

## *3.1 General*

The finite element models (FEMs) developed by the ABAQUS program of version 6.20 [41] were used to simulate the aforementioned web crippling tests of CFLDSS specimens. Four main components in the tests were modelled, namely, the steel bearing plates, the section of CFLDSS, the interactions between the steel bearing plates and CFLDSS specimen, and the boundary conditions. The measured dimensions and tested stress-strain curves of CFLDSS [37] were used in the FEMs. Also, the corners of the CFLDSS sections were accurately modelled. These will be further explained in the following sections. The results obtained from the finite element analysis (FEA) were compared with test results presented in Cai and Young [38].

### *3.2 Element types and mesh sizes*

In order to simulate the CFLDSS tubular sections, the shell element type S4R, which is a four-node doubly curved element with reduced integration and hourglass control was carefully chosen. As stated in the ABAQUS manual [41], the S4R element has six degree of freedom per node and is suitable for complex buckling behaviour. The element S4R was adopted in the FEMs in order to successfully simulate the web crippling behaviour of duplex stainless steel [30] and ferritic stainless steel [32,33] tubular members. The CFLDSS members were modelled according to the centreline dimensions of the cross-sections. The solid element type C3D8R was chosen to simulate the steel bearing plates. The steel bearing plates were defined as rigid body as the steel bearing plates in the test program [38] were fabricated by high strength steel which has a greater yield strength than those of the CFLDSS specimens. The mesh sizes ranged from 2×2 mm to 10×10 mm (length by width) in the flat portions of the cross-sections depending on the dimension of the cross-sections. Similar mesh sizes were also adopted according to sensitivity study for the FEMs of austenitic and duplex stainless steel [30] and ferritic stainless steel [32,33] tubular members subjected to web crippling. In order to account for the influence of radius at corners more accurately, a finer mesh size at these round corners was adopted [32-34, 42].

### *3.3 Material properties*

The ABAQUS [41] allows for the multi-linear stress-strain curve to be used in the input of material properties. The engineering stress-strain curves as obtained from the tensile coupon tests [37] been carried out were used accordingly. The web crippling behaviour of CFLDSS involves large in-elastic strains, therefore, it was required for the engineering stress-strain ($\sigma$-$\varepsilon$) curve to be converted to a true stress ($\sigma_{true}$) and logarithmic plastic strain ($\varepsilon_{true}^{pl}$) curve, using the following Equations (1)-(2):

$$\sigma_{true} = \sigma(1 + \varepsilon) \tag{1}$$

$$\varepsilon_{true}^{pl} = ln(1 + \varepsilon) - \frac{\sigma_{true}}{E} \tag{2}$$

where $E$ is the measured Young's modulus. The true stress and logarithmic plastic strain curve were then imitated by means of a piecewise linear stress-strain model, especially, over the strain-hardening region. Thus, the material non-linearity was included into the FEMs. The tensile material properties shown in (Table 1) [37] were assigned to the webs and flanges of the sections. The first part of the multi-linear curve represents the elastic part with the measured Young's modulus.

### 3.4 Boundary conditions

The boundary conditions in the FEMs were modelled according to the tests. Half of the CFLDSS specimens and steel bearing plates were modelled in the FEMs by assigning appropriate symmetric boundary conditions. This is due to the symmetry of the geometries and failure modes of the test specimens. In addition, the test setup and boundary conditions are symmetric for the loading conditions of IOF, ITF and IL [38]. Contact pairs were used to model the interfaces between the CFLDSS sections and the steel bearing plates, with the steel bearing plates defined as master surface while the CFLDSS sections as slave surface. The contact surfaces were defined as "hard contact" in the normal direction and not allowed to penetrate each other. Furthermore, a coefficient of 0.4 was adopted to account for the friction penalty contact in the tangential direction [32, 33]. The geometrical nonlinearity of the FEMs is considered by the NLGEOM command in ABAQUS [41].

### 3.5 Method of loading

The displacement control loading method and the general static analysis method were used in this study. The loading method used in the analysis of the FEMs of CFLDSS was the same with that used in the test program, where displacement control test method [38] was adopted. It should be noted that different analysis methods have been used for numerical models of steel members undergoing web crippling, such as general static analysis method for stainless steel tubular sections [30,33,43], quasi-static analyses with an explicit integration scheme for steel members with open sections [44,45] and quasi-static analysis with an implicit integration scheme for stainless steel members with open sections [46-48]. The cons and pros of the quasi-static analysis with different integration schemes were discussed, for example, in Yousefi *et al.* [49]. Transverse compressive load was applied by specifying a displacement to the reference point of the analytical rigid plate that simulate the steel bearing plate. Figures 2-4 illustrate the comparison of the tests and FEMs for CFLDSS specimens subjected to different concentrated interior bearing loads, for specimens IOF150×80×3.0N90, ITF100×100×3.0N90 and Specimen IL120×60×3.0N60, respectively.

## 4 Validation of finite element models

A total of 53 CFLDSS tubular sections tested by Cai and Young [38] at room temperature condition were analysed in this study to carry out verification of the FEMs. These specimens failed by web crippling under the loading conditions of IOF, ITF and IL (Tables 2-4). The Comparison of the web crippling strengths ($P_t$) per web obtained from the test program with those obtained from the finite element results ($P_{FEA,r}$) at room temperature, is shown in Tables 2-4. It can be seen that good agreement was achieved between both results for all specimens. The mean value of the $P_t/P_{FEA,r}$ for the three different loading conditions are summarized in Table 5. In general, the mean value of the $P_t/P_{FEA,r}$ for the 53 specimens is 1.08 with the corresponding coefficient of variation (COV) of 0.069. The test strengths are generally slightly higher than the predictions from the FEA. This could be due to the flat tensile material properties instead of the compressive material properties were used in the webs. The observed failure modes from the tests are well predicted by the FEA for the three different loading conditions, e.g., as illustrated in Figure 3(a)-(b). In summary, the comparisons indicated that both the failure modes and the ultimate web crippling strengths from the test program generally could be replicated by the analysis results of the developed FEMs.

## 5 Parametric study analysis and discussions

To generate numerical data for the CFLDSS tubular sections under the concentrated interior bearing loads (IOF, ITF and IL) at elevated temperatures, the validated FEMs as discussed in the previous section of this paper were used. It should be noted that there are generally two test methods for structures in fire, namely, steady state test method [26,28] and transient state test method [27,28,50]. Previous studies showed that the two test methods provided similar strength reductions at elevated temperatures, for examples, stainless steel single shear and double shear bolted connections at high temperatures [27-28]. The numerical investigation in this study generally simulate the testing procedure of steady state tests, where the specimens is heated to a pre-determined temperature level without any preloading, the specimen will then be loaded until failure while the specimen temperature is maintained. Hence, the material properties of LDSS at elevated temperature conditions were used. Similar simulation technique has been adopted in the literature, for examples, lean duplex stainless steel beams at elevated temperature [51], and steel bolted moment connections at elevated temperatures [52].

A total of 210 specimens for various temperatures including 22 (room temperature), 200, 350, 500, 600, 800 and 950 °C were analysed in the parametric study. The design of the CFLDSS tubular sections was done by considering the key parameters in the web crippling design rules [3-5] for steel tubular sections. These tubular sections include five rectangular and five square hollow sections ($H \times B \times t$). The variation of the key parameters in these sections was designed to cover a wide range, including the ratios of $h/t$ ranged from 21.0 to 145.0, $N/t$ ranged from 8.3 to 125.0 and $N/h$ ranged from 0.36 to 1.24. The section inner radius ($r$) for each specimen was designed based on the dimensions of $H$ and $B$ by referring the technical manual of the test specimen supplier. Each section was loaded with two different bearing lengths ($N$), i.e., either $N$ = 0.5$B$ or $N$ = 1.0$B$ for each loading condition (IOF, ITF or IL). Details of these sections and related parameters are presented in Table 6. The labelling system for the specimens in the parametric study is the same as that used in the test program as described in the Section 2 of this paper.

The stress-strain curves of the tensile flat coupons in the longitudinal direction of CFLDSS (grade EN 1.4162) rectangular section at elevated temperatures were used in the parametric study. These stress-strain curves were measured at elevated temperature using steady state test method by Cai and Young [26]. Due to the effect of cold-working, it should be noted that the stress-strain curves at the corner regions of the CFLDSS section may vary from those in the flat regions. The enhancements in $f_{0.2\%}$ at the corners of cold-formed sections [53] are found to be obvious at room temperature condition. Nevertheless, the material properties from corner and flat portions showed close $f_{0.2\%}$ at high temperature conditions [54]. The enhancements of the corner regions have little effects on the ultimate web crippling capacity since the web crippling failure takes place in the web for the CFLDSS tubular sections in the parametric study. In this regard, the enhancements of the strengths at the corner regions were not considered in the present study, as those studied by Zhou and Young [30] for cold-formed duplex stainless steel sections. The material properties [26], including Young's modulus ($E_T$), 0.2% proof stress ($f_{0.2\%,T}$) and ultimate strength ($f_{u,T}$), of the CFLDSS tubular section at elevated temperatures are presented in Table 7.

The same design criteria was adopted for the specimen lengths as those for the specimens in the test program [38]. The two adjacent bearing plate edges in IOF loading condition and the specimen free end to the adjacent bearing plate edge in ITF and IL loading conditions were designed with the clear distance of 1.5*H*. Altogether, 210 parametric results were generated for the web crippling of CFLDSS tubular sections at elevated temperatures under the loading conditions of IOF, ITF and IL. All these 210 CFLDSS specimens (Table 8) showed pronounce peak loads in the load-deformation curves with web crippling failure at elevated temperatures. The ultimate strengths ($P_{FEA,T}$) of the CFLDSS specimens per web at elevated temperatures are shown in Table 8.

The reduction factors ($P_{FEA,T}/P_{FEA,r}$) of web crippling strengths for CFLDSS specimens were obtained by normalizing the strengths at elevated temperatures ($P_{FEA,T}$) with that at room temperature ($P_{FEA,r}$) for the same specimen series. As shown in Figures 5-7, these reduction factors ($P_{FEA,T}/P_{FEA,r}$) were compared with those of material properties of CFLDSS (EN 1.4162) at elevated temperatures, i.e., the factors of $E_T/E_r$ and $f_{0.2,T}/f_{0.2,r}$ for the loading conditions of IOF, ITF and IL, respectively. The $E_r$ and $f_{0.2,r}$ are respectively the Young's modulus and 0.2% proof stress of CFLDSS (EN 1.4162) at room temperature (22 °C in Table 7). The specimens in these figures were differentiated by the web slenderness ratios of $h/t$. The effects of reduction factors ($E_T/E_r$ and $f_{0.2,T}/f_{0.2,r}$) on the strengths of stainless steel members at elevated temperatures were also investigated by Zhou and Young [30] for web crippling, and by Xing *et al.* [55] for plate buckling. Xing *et al.* [56] also considered the reduction factors of $f_{2,T}/f_{0.2,r}$ ($f_{2,T}$ is the stress corresponding to the 2% total strain at high temperatures) on the strengths of stainless steel members at elevated temperatures.

For the ITF and IOF loading conditions (Figures 6-7), compared to CFLDSS tubular sections with lower web slenderness in the temperatures ranged from 200 to 650 °C, the CFLDSS tubular sections with higher web slenderness, larger ratio of $h/t$, maintained better residual strengths (larger $P_{FEA,T}/P_{FEA,r}$) while the residual strengths tended to be similar in the temperatures ranged from 650 to 950 °C, as illustrated in Figures 6-7. However, similar strength reductions (Figure 5) were found for specimens under the IOF loading condition at elevated temperatures. The $E_T/E_r$ reduction factors overestimated the residual strengths of the specimens, while those of $f_{0.2,T}/f_{0.2,r}$ generally underestimated the residual strengths of the specimens in the temperatures ranged from 200 to 650 °C for the three loading conditions. Nevertheless, both $E_T/E_r$ and $f_{0.2,T}/f_{0.2,r}$ reduction factors tended to overestimate the residual strengths in the temperatures ranged from 650 to 950 °C, with the $f_{0.2,T}/f_{0.2,r}$ led to be more overestimation, for the three loading conditions (Figures 5-7).

# 6 Reliability analysis

The reliability analysis was used for assessing web crippling design rules in this study. The analysis was performed following the Commentary in the ASCE Specification [3]. The reliability index ($\beta$) is a relative measure for the design provisions in terms of reliable and probabilistically safe. A target reliability index of 2.5 was set in this study. If the calculated $\beta$ is greater than or equal to 2.5 ($\beta \geq 2.5$), the design rules are considered to be reliable and probabilistically safe. In the calculation of $\beta$, the load combination of 1.2DL + 1.6LL was used for the design rules provided by ASCE [3], NAS [39] and Zhou and Young [30], while the combination of 1.35DL + 1.5LL in European code (EC0) [57] was used for the European design rules [3, 58]. The DL and LL are the dead load and live load respectively. The DL/LL was set as 0.2 in ASCE [3]. The proposed mean value and COV of the material factor are respectively $M_m$ = 1.10 and $F_m$ = 1.00; and those of fabrication factor are $V_M$ = 0.10 and $V_F$ = 0.05 in Section 6.2 of ASCE [3]. Furthermore, a correction factor ($C_P$) as specified in ASCE [3] was used to consider the influence of limited test and numerical results. The corresponding reliability index ($\beta$) was calculated by the resistance factor ($\phi$) specified in those design rules. The reliability analysis of the design rules is discussed in the later sections of this paper.

# 7 Current design rules and assessments

## *7.1 General*

Due to the complexity of the theoretical analysis, the existing design rules found in most specifications for web crippling of cold-formed steel structures are semi-empirical in nature. It should be noted that the web crippling design rules in the current international stainless steel specifications (ASCE [3]; AS/NZS [4] and EC3-1.4 [5]) are mainly adopted from those of carbon steel design specifications. The applicability of these design rules should be assessed due to the fundamental difference of stress-strain curves between carbon steel and stainless steel in nature. In addition, it should be noted that these design rules may not sufficiently account for the sections outside the range of variables in the FEA in this study, and they are only provided for room temperature condition, but not for elevated temperature conditions. However, the assessments were made for the suitability of these design rules (ASCE [3]; AS/NZS [4] and EC3-1.4 [5]) for the predictions of the nominal web crippling strengths (unfactored design strengths) per web of the CFLDSS tubular sections at elevated temperatures subjected to concentrated interior bearing loads (IOF, ITF and IL).

Apart from the stainless steel design specifications mentioned above, the unified design equation for different loading conditions (including IOF and ITF) specified in the NAS [39] was also used in this study. It should be noted that the unified design equation in NAS [39] is provided for cold-formed carbon steel structural members at room temperature condition. When calculating the nominal strengths, the reduced material properties (Table 7) of CFLDSS due to elevated temperatures were used.

The modification of the unified design equation in NAS [39] was done by Zhou and Young [30] by proposing new sets of coefficients. These new coefficients in the unified design equation was proposed for web crippling design of cold-formed duplex stainless steel (EN 1.4462) tubular sections at elevated temperatures under different loading conditions, including IOF and ITF in this study. The modified unified design equations were also adopted in the present study.

### *7.2 Design rules*

The detailed discussion for the differences of the design rules in current stainless steel design specifications ASCE [3]; AS/NZS [4] and EC3-1.4 [5]) are given by Cai and Young [37]. The ASCE Specification [3] and the AS/NZS Standard [4] provide similar design rules. Hence, the design rules in the ASCE [3] were adopted, where the web crippling design rules are specified in Section 3.3.4 of the ASCE Specification [3]. Since web crippling design rules are not provided in the EC3-1.4 [5], hence, in the strength calculations predicted by Eurocode, those specified in the EC3-1.3 [58] for cold-formed steel members, where the design for "Local transverse forces" in Section 6.1.7.3 of the EC3-1.3 [58] was used. Furthermore, the unified design equation (Equation (3-1)) specified in Section G5 of the NAS [39] for web crippling strength cold-formed carbon steel structural members was used.

$$P = Ct^2 f_{0.2} \sin\theta \,(1 - C_R\sqrt{\frac{r}{t}})(1 + C_N\sqrt{\frac{N}{t}})(1 - C_h\sqrt{\frac{h}{t}}) \qquad (3\text{-}1)$$

where $P$ = nominal web crippling strength per web, $C$ = overall web crippling coefficient; $C_R$ = inside corner radius coefficient; $C_N$ = bearing length coefficient; $C_h$ = web slenderness coefficient. Table 9 shows the coefficients and the application limits specified in NAS [39] for Equation (3). Also, the modified design equation proposed by Zhou and Young [30] for cold-formed duplex stainless steel (EN 1.4462) tubular sections at elevated temperatures are shown in Equation (4). The coefficients and the application limits for Equation (3-2) are also presented in Table 9.

$$P = Ct^2 f_{0.2,T} \sin\theta \,(1 - C_R\sqrt{\frac{r}{t}})(1 + C_N\sqrt{\frac{N}{t}})(1 - C_h(\frac{f_{0.2,T}}{E_T})\sqrt{\frac{h}{t}}) \qquad (3\text{-}2)$$

where $f_{0.2,T}$ and $E_T$ are the yield stress (0.2% proof stress) and the elastic modulus at a given temperature in degree Celsius (°C), respectively.

It should be noted that the loading condition of IL is not provided in ASCE [3], NAS [39], and Zhou and Young [30]. For the purpose of comparison and assessment, the designs for the loading conditions of both IOF and ITF were calculated for the EL loading condition in the nominal strength predictions by ASCE [3], NAS [39] and Zhou and Young [30] in the current study.

### *7.3 Assessment of current predictions*

The ultimate strengths ($P_{FEA,T}$) per web at elevated temperatures were compared with those predicted by the current design specifications for CFLDSS tubular sections subjected to the loading conditions of IOF, ITF and IL, respectively, as shown in Figures 8-10. Tables 10-12 summarize the comparisons, where the comparisons were divided at each temperature level in each table. In the calculation of strength predictions, the material properties in the design equations were substituted by the material properties at elevated temperatures. It should be noted that the material properties ($E_T$ and $f_{0.2,T}$) in Table 7 at elevated temperatures were used as the corresponding stress-strain curves were used for the CFLDSS specimens in the parametric study.

For the CFLDSS specimens subjected to IOF loading condition at elevated temperatures (see Figure 8), the predictions by the ASCE [3] were conservative for all the specimens at room temperature condition (i.e., 22 °C), unconservative for all the specimens in the temperatures ranged from 800 to 950 °C, as shown in Figure 8(a). The predictions by EC3-1.3 [58] were overall conservative for all the specimens at elevated temperatures (see Figure 8(b)). This is due to the reason that that the web slenderness ratio ($h/t$) and the actual bearing lengths ($N$) are not considered in the design provisions of EC3-1.3 [58]. Note that the CFLDSS specimen sections had different web slenderness ($h/t$) and were loaded by steel plates with different bearing lengths ($N$). On the contrary to those predictions by the ASCE [3], the predictions by the NAS [39] (see Figure 8(c)), were generally unconservative for all the specimens at elevated temperatures expect for at the temperatures level of 950 °C. The predictions by Zhou and Young [30] overall provided better predictions than those predicted by NAS [39], especially for the webs with 16.8 < *h*/*t* < 60 at elevated temperatures, as the ratios of $P_{FEA,T}/P_{Z\&Y}$ centralized around 1.0 (see Figure 8(d)).

For the CFLDSS specimens subjected to ITF loading condition at elevated temperatures (see Figure 9), the predictions by the ASCE [3], see Figure 9(a), were conservative for all the specimens at room temperature (22 °C) condition; while in the temperatures ranged from 200 to 950 °C, the predictions were unconservative for specimens with stockier webs (*h*/*t* = 16.8 and 21.0) and became conservative for the specimens with more slender webs (*h*/*t* = 120 and 145). Similar to those predictions for IOF loading condition, the predictions by EC3-1.3 [58] were overall conservative for all the specimens at elevated temperatures, as shown in Figure 9(b). On the contrary to those predictions by the ASCE [3], the predictions by the NAS [39], see Figure 9(c), were unconservative for all the specimens at room temperature condition, and also unconservative in the temperature ranged from 200 to 800 °C; the predictions were generally conservative for specimens with more slender webs at the temperature level of 950 °C. The predictions by Zhou and Young [30] generally provided similar predictions as those by NAS [39], but better predictions for the specimens at the temperatures ranged from 200 to 800 °C as the ratios of $P_{FEA,T}/P_{Z\&Y}$ were centralized around 1.0, see Figure 9(d).

For the CFLDSS specimens subjected to IL loading condition at elevated temperatures, the comparisons from different provisions are shown in Figure 10. As mentioned previously, both ITF and IOF design rules were used for the predictions of specimens under IL loading condition by the ASCE [3], NAS [39] and Zhou and Young [30]. The predictions from these provisions [3, 30, 39] by using the design rules for IOF and ITF loading conditions were distinguished by the superscript of "#" and "^", respectively. For the predictions by the ASCE [3], it is shown that the predictions of $P_{ASCE}^{\#}$ and $P_{ASCE}^{\wedge}$ were generally conservative for all the specimens in the temperatures ranged from 22 to 500 °C, but unconservative in the temperatures ranged from 800 to 950 °C; as shown in Figure 10(a)-(b). Similar to those predictions for IOF and IL loading conditions, the predictions by EC3-1.3 [58] were overall conservative for all the specimens at elevated temperatures (see Figure 10(c)). The predictions of $P_{NAS}^{\#}$, see Figure 10(d), were generally unconservative and conservative for the specimens at room temperature and the temperature level of 950 °C, respectively; however, the predictions of $P_{NAS}^{\wedge}$, see Figure 10(e), were generally unconservative for all the specimens at elevated temperatures except for those at the temperature level of 950 °C. The predictions of $P_{Z\&Y}^{\#}$ (see Figure 10(f)) and $P_{Z\&Y}^{\wedge}$ (see Figure 10(g)) by Zhou and Young [30] generally showed similar trend, namely, as the web slenderness of *h*/*t* increased, the conservative predictions of $P_{Z\&Y}^{\#}$ and $P_{Z\&Y}^{\wedge}$ tended to be unconservative at elevated temperatures.

The mean value of FEA strength-to-predicted strength with the corresponding COV for each temperature lever and at elevated temperatures (22 ~ 950 °C) were illustrated in Tables 10-12 for the loading conditions of IOF, ITF and IL, respectively. For IOF loading condition at elevated temperatures (see Table 10), the mean values for the predictions by ASCE [3], NAS [39] and Zhou and Young [30] are 0.99, 0.91 and 0.96, respectively, with the corresponding COV of 0.243, 0.169 and 0.132. However, the predictions by NAS [39] are not reliable due to the values of $\beta$ = 1.79 that is smaller than 2.5; the predictions by EC3-1.3 [58] are very conservative but reliable. For ITF loading condition at elevated temperatures (see Table 11), the mean values for the predictions by ASCE [3], and NAS [39] are 1.00 and 0.77, while these predictions are not reliable due to the corresponding $\beta <$ 2.5; Both the predictions by Zhou and Young [30] and EC3-1.3 [58] are reliable, while the EC3-1.3 [58] provided very conservative predictions. For IL loading condition at elevated temperatures (see Table 12), by using the IOF and ITF design rules, the predictions by ASCE [3] and Zhou and Young [30] are overall conservative, and these predictions are reliable except for the predictions of $P^{\wedge}_{ASCE}$; however, both the predictions by using the IOF and ITF design rules for NAS [39] are not reliable. Similar to those of the two loading conditions at elevated temperatures, very conservative and reliable predictions by EC3-1.3 [58] were found.

# 8 Proposed design rules and assessments

## *8.1 General*

As discussed in the previous section of this paper, the predictions by the NAS [39] were generally unconservative and not reliable while those by EC3-1.3 [58] were very conservative and reliable for the web crippling of CFLDSS tubular sections at elevated temperatures under the loading conditions of IOF, ITF and IL. The ASCE [3] provided not reliable predictions for the loading condition of ITF, and the loading condition of IL when the design rule for ITF was adopted. The modified unified design equation proposed by Zhou and Young [30] for cold-formed duplex stainless steel at elevated temperatures provided reliable predictions but slightly unconservative predictions for the loading condition of IOF and conservative predictions for the loading conditions of IL. Note that the design for the IL loading condition was not provided in the modified equation [30]. Hence, investigation was made for the web crippling design of CFLDSS tubular sections at elevated temperatures, under the loading conditions of IOF, ITF and IL in this study.

The Direct Strength Method (DSM) [59] is an alternative way to determine the strength of cold-formed steel members. Compared to the conventional design method, DSM could be more suitable when the effective area of a slender section is difficult to find out. The DSM has been developed and documented in the design specifications, such as the NAS [39] for the design of cold-formed steel beams and columns. It should be noted that the current DSM in design specifications does not provide design rules for web crippling design of cold-formed steel members. Investigations of DSM for the web crippling design of cold-formed steel members have been conducted by researchers in the past few years, such as for cold-formed steel open sections conducted by Keerthan *et al*. [60] and Natário *et al*. [61,62] and for cold-formed ferritic stainless steel rectangular and square hollow sections conducted by Li and Young [32,33]. A more recent study by Cai and Young [63] extended the DSM for the web crippling design of CFLDSS tubular sections under the loading conditions of IOF, ITF and IL. So far, these DSM methods [32-33, 60-62] for web crippling design were only proposed for the design at room temperature condition, but not for elevated temperature conditions. To extend its application to web crippling design of CFLDSS tubular sections at elevated temperatures, efforts on the DSM modifications are made in this study.

### *8.2 Modified DSM*

The presented format of DSM in Li and Young [32] and Cai and Young [63] for web crippling design of stainless steel sections at room temperature is illustrated in Equation (4), where different sets of coefficient for $a$, $b$, $n$, $\gamma$ and $\lambda_k$ in Equation (4) were proposed depending on stainless steel grades and loading conditions. The two different types of web crippling failure for cold-formed stainless steel square and rectangular hollow sections are, web buckling, where the web crippling capacity mainly depends on the stiffness of the material, and yielding in the web, where the web crippling capacity mainly depends on the yield strength of the material [30]. As it was earlier presented in Figures 5-7, the web crippling strength reduction factors ($P_{FEA,T}/P_{FEA,r}$), 0.2% proof stress ($f_{0.2,T}/f_{0.2,r}$) and Young's modulus ($E_T/E_r$) of CFLDSS sections depicted similar reduction trends at elevated temperature for different loading conditions. Similar to Zhou and Young's proposal as shown in Equation (3-2), the factor $\chi$ as shown in Equation (5) was proposed to account for the effects of 0.2% proof stress ($f_{0.2,T}$) and Young's modulus ($E_T$) of the material properties at elevated temperatures. It should be noted that the factors due to the effects of $f_{2,T}$ at elevated temperatures were also considered by Xing *et al.* [56] for plate buckling of stainless steel. To be consistent with the design at room temperature condition, the $f_{0.2,T}$ was considered in this study. The CFLDSS tubular sections subjected to web crippling ($P_{DSM,T}$) at elevated temperatures could then be calculated by $\chi P_{DSM}$, as seen in Equation (6).

$$P_{DSM} = \begin{cases} \gamma P_{y,T} & \lambda \le \lambda_k \\ a\left[1 - b\left(\frac{P_{cr,T}}{P_{y,T}}\right)^n\right]\left(\frac{P_{cr,T}}{P_{y,T}}\right)^n P_{y,T} & \lambda > \lambda_k \end{cases} \tag{4}$$

$$\chi = \frac{1}{0.0036}\frac{f_{0.2,T}}{E_T} \tag{5}$$

$$P_{DSM,T} = \chi P_{DSM} \tag{6}$$

where $\lambda = \sqrt{P_{y,T}/P_{cr,T}}$ is the web crippling slenderness ratio. The $P_{cr,T}$ and $P_{y,T}$ are respectively the nominal bearing strengths per web for buckling and yielding at elevated temperatures.

Generally, a computer software is required for the DSM to compute the nominal bearing strength for buckling at room temperature, e.g., the DSM proposed by Natário *et al.* [61,62]. Nevertheless, this is not essential for the calculation of $P_{cr,T}$ in Equation (4). Alternatively, the calculations of $P_{cr,T}$ and $P_{y,T}$ could be done manually by referring Clause 5.13 of the AS 4100 [64], as recommended and adopted by Li and Young [32,33] for room temperature condition, and shown in the following Equations (7)-(11). It should be noted that these equations are provided for the design at room temperature condition [64], but not for elevated temperature conditions. Therefore, the 0.2% proof stress ($f_{0.2,r}$) at room temperature was replaced by those ($f_{0.2,T}$) at elevated temperatures in these calculations.

$$P_{cr} = \alpha_c t N_m f_{0.2,T} \tag{7}$$

where $\alpha_c$ is the slenderness reduction factor as specified in Clause 6.3.3 of the AS 4100 [64], $N_m$ is the mechanism length for the loading conditions of IOF, ITF and IL, which could be determined by the following Equation (8):

$$N_m = N + 5R + h \tag{8}$$

where $R$ is the outer corner radius.

$$P_y = \alpha_p t N_m f_{0.2,T} \tag{9}$$

For IOF, ITF and IL loading conditions:

$$\alpha_p = \frac{0.5}{k_s}\left[1 + \left(1 - \alpha_{pm}^2\right)\left(1 + \frac{k_s}{k_v} - \left(1 - \alpha_{pm}^2\right)\frac{0.25}{k_v^2}\right)\right] \tag{10}$$

where $k_s = 2R/t - 1$, $\alpha_{pm} = 1/k_s + 0.5/k_v$ and $k_v = h/t$.

In this study, different values of $a$, $\lambda_k$ and $\gamma$ similar to those recommended by Li and Young [32,33] and Cai and Young [63] are proposed for different loading conditions. However, the constant coefficients of $b$ = 0.20 and $n$ = 0.60 as well as resistance factor of $\phi$ = 0.80 are proposed irrespective of different loading conditions. These coefficients (see Table 13) are proposed for the web crippling design at elevated temperature conditions, and also applicable for CFLDSS square and rectangular hollow sections having stiffened or partially stiffened flanges with the limits for $10 \le h/t \le 145$, $r/t \le 2.0$, $N/t \le 150$ and $N/h \le 1.5$. The coefficients for the Equation (4) were calibrated against the 210 numerical results (Table 8) at elevated temperatures in this study. In addition, the coefficients for the Equation (4) were also calibrated against the 58 test results [37] of CFLDSS sections at room temperature under the loading conditions of IOF, ITF and IL.

### *8.3 Assessment of modified DSM predictions*

The newly proposed coefficients (Table 13), as shown in Figures 11(a)-(c) for the loading conditions of IOF, ITF and IL, respectively, were used to calculate the ultimate strengths ($P_{FEA,T}$) per web at elevated temperatures and they are compared with those predicted by the modified DSM ($P_{DSM,T}$). These comparisons were also summarized in Tables 10-12, as those comparisons for the current predictions presented in Section 7.3.

As it was shown, the modified DSM ($P_{DSM,T}$) for the web crippling strengths of CFLDSS tubular sections at elevated temperature generally provided conservative predictions. However, in contrast to those predictions by Zhou and Young [30] (see Figures 8(d), 9(d) and 10(g)) and some other predictions that showed the reduction trends with the increment of $h/t$ at each temperature level, the effects of $h/t$ on the predictions by the modified DSM at each temperature level were to some certain level eliminated, except for those at the temperature level of 950 °C. As shown in Tables 10-12, the predictions by the modified DSM ($P_{DSM,T}$) are conservative at each temperature level for the three loading conditions, except for that at room temperature (22 °C) for the loading conditions of IOF, ITF and IL. For each loading conditions, the overall conservative predictions are mainly due to the very conservative predictions for the strengths at the temperature levels of 650 and 950 °C as shown in the mean values of $P_{FEA,T}/P_{DSM,T}$ (see Tables 10-12). These data are further illustrated in Figures 12-14. The comparisons of the numerical results at elevated temperatures with the DSM curves (using Equation (4)) for the loading conditions of IOF, ITF and IL, respectively are shown in Figures 12-14. In each figure, the ratio of $(1/\chi)(P_{FEA,T}/P_{y,T})$ were plotted against the web crippling slenderness ratio of $(P_{y,T}/P_{cr,T})^{0.5}$.

The reliability analysis conducted for the ultimate strength ($P_{DSM,T}$) predicted by using the modified DSM are reliable for all the three loading conditions at elevated temperatures. The previously-mentioned values for the material factor and fabrication factor in Section 6 were all adopted. Furthermore, the load combination of 1.2DL + 1.6LL was used. The resistance factor of 0.8 (see Table 11) was used to compute the reliability indices ($\beta$). It can be testified that the predictions by the modified DSM are reliable as proved by the values of reliability indices above the target value of 2.5 ($\beta$ > 2.5).

As shown in Tables 14-16 , the web crippling strengths ($P_t$) of CFLDSS square and rectangular hollow sections at room temperature (22 °C) conducted by Cai and Young [38] were also used to compare with the strengths ($P_{DSM,T}$) predicted by using the proposed DSM equation, Equation (6), for elevated temperature conditions. The purpose of these comparisons is to show that the predictions from the proposed design equations are safe and reliable for the available test data. Same values of the coefficients in Tables 13 for CFLDSS tubular sections at elevated temperatures were adopted for the calculation. The same factors and load combination used for the reliability analysis mentioned earlier in the previous paragraph were adopted. It is seen that the predicted strengths are overall conservative and reliable for the three loading conditions (IOF, ITF and IL), as proved by the mean values of $P_t/P_{DSM,T}$ above 1.00 with their corresponding reliability indices ($\beta$) above 2.5.

## 9 Conclusions

Non-linear finite element models (FEMs) were developed for the web crippling of cold-formed lean duplex stainless steel (CFLDSS) square and rectangular hollow sections under the concentrated interior bearing loads, namely, the loading conditions of Interior-One-Flange (IOF), Interior-Two-Flange (ITF) and Interior Loading (IL). After successful verification of the FEMs against with the 36 test results, an extensive parametric study of 210 CFLDSS tubular sections at elevated temperatures was performed. These sections were subjected to web crippling under the three concentrated interior bearing loads at different temperatures ranged from 22 (room temperature) to 950 °C. The CFLDSS specimens were carefully designed to cover a wide range of the key parameters, including the ratios of flat web height ($h$) to thickness ($t$) with $h/t$ ranged from 21.0 to 145.0, bearing length ($N$) to web thickness ($t$) with $N/t$ ranged from 8.3 to 125.0, as well as the ratio of $N/h$ ranged from 0.36 to 1.24.

The appropriateness of the web crippling design rules in the current international specifications (ASCE [3], AS/NZS [4], NAS [39] and EC3-1.3 [58]) has been examined by comparing their ultimate strengths predictions with those obtained from the finite element analysis for CFLDSS at elevated temperatures. In these codified calculations, the material properties at room temperature condition were substituted by those at elevated temperatures. Furthermore, the modified unified design equation in the literature for web crippling of cold-formed duplex stainless steel at elevated temperatures was also used. The reliability of the design provisions was assessed by reliability analysis. It was found that the predictions by the predictions by the NAS were generally unconservative and not reliable while those by EC3-1.3 [58] were very conservative and reliable for the web crippling of CFLDSS tubular sections at elevated temperatures under the loading conditions of IOF, ITF and IL. The ASCE and AS/NZS provided not reliable predictions for the loading condition of ITF, and the loading condition of IL when the design rule for ITF was adopted. The modified unified design equation provided conservative and reliable predictions, except for the slightly unconservative predictions for the loading condition of IOF.

New design method is proposed, including a new equation that considering the effects of 0.2% proof stress and Young's modulus at elevated temperatures and the modified Direct Strength Method (DSM) by proposing new sets of coefficients for the loading conditions of IOF, ITF and IL. The proposed design method were calibrated against the numerical results from parametric study. It is shown that the predictions by using the new method are generally conservative and reliable for CFLDSS square and rectangular hollow sections at elevated temperatures under the three loading conditions. In addition, the web crippling test results of CFLDSS square and rectangular hollow sections at room temperature in literature were also compared with the predicted strengths obtained using the proposed method. It is shown that the predicted strengths are also generally conservative and reliable for the web crippling tests. Therefore, the newly proposed method is applicable for web crippling (loading conditions of IOF, ITF and IL) design of CFLDSS square and rectangular hollow sections at elevated temperatures with limits of $21 \leq h/t \leq 145$, $r_i/t \leq 2.0$, $N/t \leq 125$ and $N/h \leq 1.25$. The flanges of the CFLDSS tubular sections are stiffened or partially stiffened that unfastened to the supports.

**Acknowledgement**

The first author wishes to acknowledge the support provided by the Chinese National Engineering Research Centre for Steel Construction (Hong Kong Branch) at the Hong Kong Polytechnic University which is funded by the Innovation and Technology Fund administrated by the Innovation and Technology Commission of the Commissioner of the Government of Hong Kong SAR.

## References

[1] Ronald, L.P., Clara, H., Doris, M.E., Paulo, R.R., Angelo, F.P. A Short Review on Wrought Austenitic Stainless Steels at High Temperatures: Processing, Microstructure, Properties and Performance. Materials Research 2007; 10 (4): 453-460.

[2] Gardner, L. Stability and design of stainless steel structures – Review and outlook, Thin-Walled Structures 2019; 141: 208-216.

[3] ASCE. Specification for the design of cold-formed stainless steel structural members. American Society of Civil Engineers (ASCE), ASCE Standard, SEI/ASCE-8-02, Reston, Virginia, 2002.

[4] AS/NZS. Cold-formed stainless steel structures. AS/NZS 4673:2001, Australian/New Zealand Standard (AS/NZS), Standards Australia, Sydney, Australia, 2001.

[5] EC3-1.4. Eurocode 3. Design of steel structures - Part 1.4: General rules - Supplementary rules for stainless steels. EN 1993-1-4:2006+A1:2015, Brussels, Belgium, European Committee for Standardization, 2015.

[6] Huang, Y., Young, B. Material properties of cold-formed lean duplex stainless steel sections. Thin-Walled Structures 2012; 54: 72-81.

[7] Saliba, N., Gardner, L. Cross-section stability of lean duplex stainless steel welded I-sections. Journal of Constructional Steel Research 2013; 18: 1-14.

[8] Huang, Y., Young, B. Experimental and numerical investigation of cold-formed lean duplex stainless steel flexural members. Thin-Walled Structures 2014; 73: 216-228.

[9] Huang, Y., Young, B. Tests of pin-ended cold-formed lean duplex stainless steel columns. Journal of Constructional Steel Research 2013; 82: 203-215.

[10] Zhao, O., Rossi, B., Gardner, L., Young, B. Behaviour of structural stainless steel cross-sections under combined loading - Part I: Experimental study. Engineering Structures 2015; 89: 236-246.

[11] Zhao, O., Rossi, B., Gardner, L., Young, B. Behaviour of structural stainless steel cross-sections under combined loading - Part II: Numerical modelling and design." Engineering Structures 2015; 89: 247-259.

[12] Saliba, N., Gardner, L. Experimental study of the shear response of lean duplex stainless steel plate girders. Engineering Structures 2013; 46: 375-391.

[13] Saliba N., Real, E., Gardner, L. Shear design recommendations for stainless steel plate girders." Engineering Structures 2014; 59: 220-228.

[14] Cai, Y., Young, B. Structural behavior of cold-formed stainless steel bolted connections. Thin-Walled Structures 2014; 83: 147-156.

[15] Design of steel structures—Part 1.4: general rules— supplementary rules for stainless steels. EN 1993-1-4. Brussels: European Committee for Standardization; 2006.

[16] Feng, M., Wang, Y.C., Davies, J.M. Structural behaviour of cold-formed thin-walled short steel channel columns at elevated temperatures - Part 1: experiments. Thin-Walled Structures 2003; 41 (6): 543-570.

[17] Feng, M., Wang, Y.C., Davies, J.M. Structural behaviour of cold-formed thin-walled short steel channel columns at elevated temperatures - Part 2: design calculations and numerical analysis. Thin-Walled Structures 2003; 41 (6): 571-594.

[18] Chen, J., Young, B. Design of high strength steel columns at elevated temperatures, Journal of Constructional Steel Research 2008; 64 (6): 689-703.

[19] Ranawaka1, T., Mahendran, M. Numerical modelling of light gauge cold-formed steel compression members subjected to distortional buckling at elevated temperatures. Thin-Walled Structures 2010; 48: 334-344.

[20] Cheng, S., Li, L.-Y., Kim, B. Buckling analysis of cold-formed steel channel-section beams at elevated temperatures. Journal of Constructional Steel Research 2015; 104: 74-80.

[21] Landesmanna, A., Camotim, D. Distortional failure and DSM design of cold-formed steel lipped channel beams under elevated temperatures. Thin-Walled Structures 2016; 98: 75-93.

[22] Li, H.-T., Young, B. Cold-formed high strength steel SHS and RHS beams at elevated temperatures. Journal of Constructional Steel Research 2019; 158: 475-485.

[23] Gardner, L., Insaustia, A., Ng, K.T., Ashraf, M. Elevated temperature material properties of stainless steel alloys. Journal of Constructional Steel Research 2010; 66 (5): 634-647

[24] Chen, J., Jin, W.-L. Behaviour of cold-formed stainless steel beams at elevated temperatures. Journal of Zhejiang University-SCIENCE A 2008; 9: 1507-1513.

[25] Feng, R., Young, B. Design of cold-formed stainless steel tubular joints at elevated temperatures. Engineering Structures 2012; 35: 188-202

[26] Cai, Y., Young, B. Behavior of cold-formed stainless steel single shear bolted connections at elevated temperatures. Thin-Walled Structures 2014; 75: 63-75.

[27] Cai, Y., Young, B. Transient state tests of cold-formed stainless steel single shear bolted connections. Engineering Structures 2014; 81: 1-9.

[28] Cai, Y., Young, B. High temperature tests of cold-formed stainless steel double shear bolted connections. Journal of Constructional Steel Research 2015; 104: 49-63.

[29] Cai, Y., Young, B. Bearing resistance design of stainless steel bolted connections at ambient and elevated temperatures. Steel and Composite Structures, An International Journal 2018; Techno-Press, 29(2): 273-286.

[30] Zhou, F., Young, B. Web crippling behaviour of cold-formed duplex stainless steel tubular sections at elevated temperatures. Engineering Structures 2013; 57: 51-62.

[31] Zhou, F., Young, B. Cold-formed high-strength stainless steel tubular sections subjected to web crippling. Journal of Structural Engineering 2007; 133(3): 368-377.

[32] Li, H-T., Young, B. Cold-formed ferritic stainless steel tubular structural members subjected to concentrated bearing loads. Engineering Structures 2017; 145: 392-405.

[33] Li, H-T., Young, B. Web crippling of cold-formed ferritic stainless steel square and rectangular hollow sections. Engineering Structures 2018; 176: 968-980.

[34] Bock, M., Arrayago, I., Real, E., Mirambell, E. Study of web crippling in ferritic stainless steel cold formed sections. Thin-Walled Structures 2013; 69: 29-44.

[35] dos Santos, G.B., Gardner L., Kucukler M. Experimental and numerical study of stainless steel I-sections under concentrated internal one-flange and internal two-flange loading. Engineering Structures 2018; 175: 355-370.

[36] dos Santos, G.B., Gardner L. Testing and numerical analysis of stainless steel I-sections under concentrated end-one-flange loading. Journal of Constructional Steel Research 2019; 157: 271-281.

[37] Cai, Y., Young, B. Web crippling of lean duplex stainless steel tubular sections under concentrated end bearing loads. Thin-Walled Structures 2019; 134: 29-39.

[38] Cai, Y., Young, B. Cold-formed lean duplex stainless steel tubular members under concentrated interior bearing loads. Journal of Structural Engineering 2019; ASCE. 145(7): 04019056.

[39] North American Specification (NAS) North American Specification for the design of cold-formed steel structural members. AISI S100–16, Washington D. C., USA: American Iron and Steel Institute (AISI); 2016.

[40] Zhou, F., Young, B. Web crippling of cold-formed stainless steel tubular sections. Advances in Structural engineering 2008; 11(6): 679-691.

[41] ABAQUS. Analysis User's Manual, ABAQUS, Inc., Version 6.20, 2019.

[42] Lian, Y., Uzzaman, A., Lim, J.B.P., Abdelal, G., Nash, D., Young, B. Effect of web holes on web crippling strength of cold-formed steel channel sections under end-one-flange loading condition - Part I: Tests and finite element analysis. Thin-Walled Structures 2016; 107: 443-452.

[43] Cai, Y., Young, B. Design of lean duplex stainless steel tubular sections subjected concentrated end-bearing loads. Journal of Structural Engineering 2021; 147(4), 04021009.

[44] Natario, P., Silvestre, N. and Camotim, D. Computational modelling of flange crushing in cold-formed steel sections. Thin-Walled Structures 2014; 84: 393-405.

[45] Natario, P., Silvestre, N. and Camotim, D. Web crippling failure using quasi-static FE models. Thin-Walled Structures 2014; 84: 34-49.

[46] Yousefi, A. M., Lim, J.B.P. and Clifton, G.C. Cold-formed ferritic stainless steel unlipped channels with web openings subjected to web crippling under interior-two-flange loading condition. I: Tests and finite element model validation. Thin-Walled Structures 2017; 116: 333-341.

[47] Yousefi, A. M., Lim, J.B.P. and Clifton, G.C. Cold-formed ferritic stainless steel unlipped channels with web openings subjected to web crippling under interior-two-flange loading condition. II: Parametric study and design equations. Thin-Walled Structures 2017; 116: 342-356.

[48] Yousefi, A. M., Lim, J.B.P. and Clifton, G.C. Web bearing capacity of unlipped cold-formed ferritic stainless steel channels with perforated web subject to end-two-flange (ETF) loading. Engineering Structures 2017; 152: 804-818.

[49] Yousefi, A. M., Lim, J.B.P. and Clifton, G.C. Web Crippling Behavior of Unlipped Cold-Formed Ferritic Stainless Steel Channels Subject to One-Flange Loadings. Journal of Structural Engineering 2018; 144(8): 04018105.

[50] Roy, K., Lim, J.B.P., L., Lau, H.H., Yong, P.M. Clifton, G.C., Johnston R.P.D., Wrzesien A. and Mei, C.C. Collapse behaviour of a fire engineering designed single-storey cold-formed steel building in severe fires. Thin-Walled Structures 2019; 142: 340-357.

[51] Huang, Y. and Young, B. Structural performance of cold-formed lean duplex stainless steel beams at elevated temperatures. Thin-Walled Structures 2018; 129: 20-27.

[52] Lim, J.B.P. and Young, B. Effects of elevated temperatures on bolted moment-connections between cold-formed steel members. Engineering Structures 2007; 29 (10): 2419-2427.

[53] Gardner, L., Nethercot, D.A. Experiments on stainless steel hollow sections—Part 1: Material and cross-sectional behavior. Journal of Constructional Steel Research 2004; 60(9): 1291-1318.

[54] Ala-Outinen T. Fire resistance of austenitic stainless steels Polarit 725 (EN 1.4301) and Polarit 761 (EN 1.4571). VTT Research Notes 1760. Espoo, Finland, 1996.

[55] Xing, Z., Kucukler, M. and Gardner, L. Local buckling of stainless steel plates in fire. Thin-Walled Structures 2020; 148: 106570.

[56] Xing, Z., Kucukler, M. and Gardner, L. Local buckling of stainless steel I-sections in fire: Finite element modelling and design. Thin-Walled Structures 2021; 161: 107486.

[57] EC0. Eurocode 0: basis of structural design. EN 1990:2002+A1:2005. Brussels, Belgium: European committee for standardization; 2005.

[58] EC3-1.3. Eurocode 3: Design of steel structures - Part 1-3: General rules - Supplementary rules for cold-formed members and sheeting. EN 1993-1-3, Brussels, Belgium: European committee for standardization; 2006.

[59] Schafer, B.W. Review: The Direct Strength Method of cold-formed steel member design. Journal of Constructional Steel Research 2008; 64(7-8): 766-778.

[60] Keerthan, P., Mahendran, M., Steau, E. Experimental study of web crippling behaviour of hollow flange channel beams under two flange load cases. Thin-Walled Structure 2014; 85: 207-19.

[61] Natário, P., Silvestre, N., Camotim, D. Direct strength prediction of web crippling failure of beams under ETF loading. Thin-Walled Structures 2016; 2(98): 360-74.

[62] Natário, P., Silvestre, N., Camotim, D. Web crippling of beams under ITF loading: a novel DSM-based design approach. Journal of Constructional Steel Research 2017; 128: 812-24.

[63] Cai, Y., Young, B. Web crippling design of lean duplex stainless steel tubular members under interior loading conditions. Engineering Structures 2021 (In press).

[64] Australian Standard (AS). Steel structures. AS 4100, Sydney, Australia: Standards Australia; 1998.

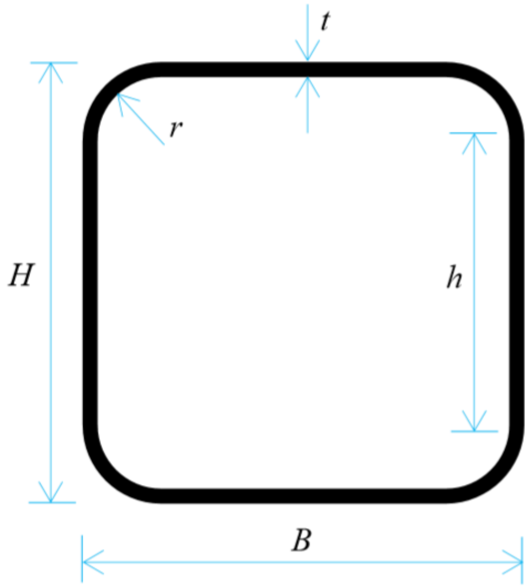


**Figure 1:** Definition of symbols in a tubular section

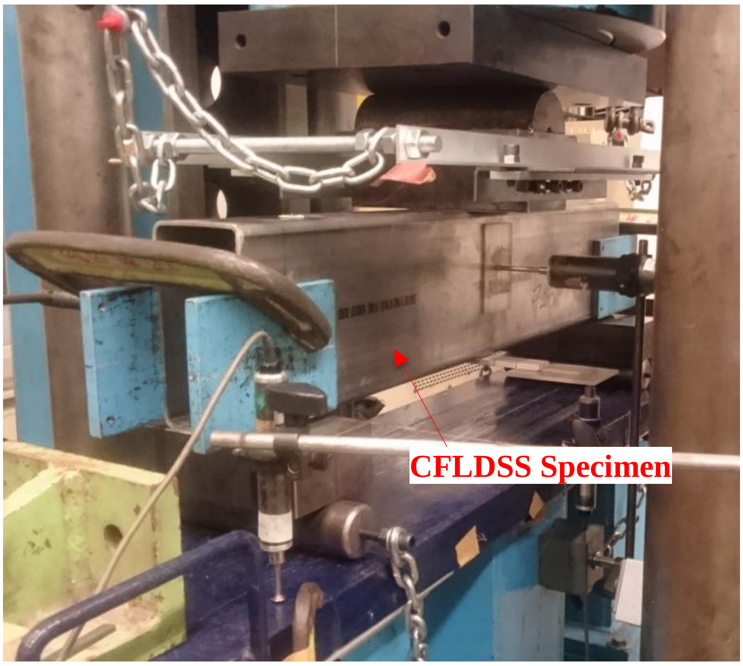

(a) Specimen in the test

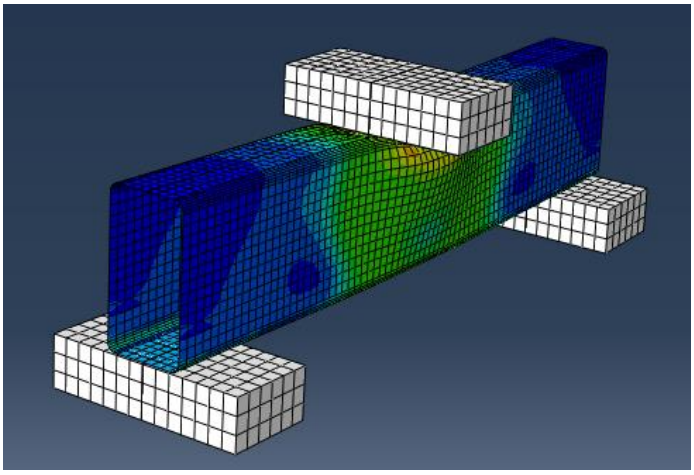
(b) Specimen in finite element analysis

**Figure 2:** Comparison of test and numerical model for Specimen IOF150×80×3.0N90


(a) Specimen in the test

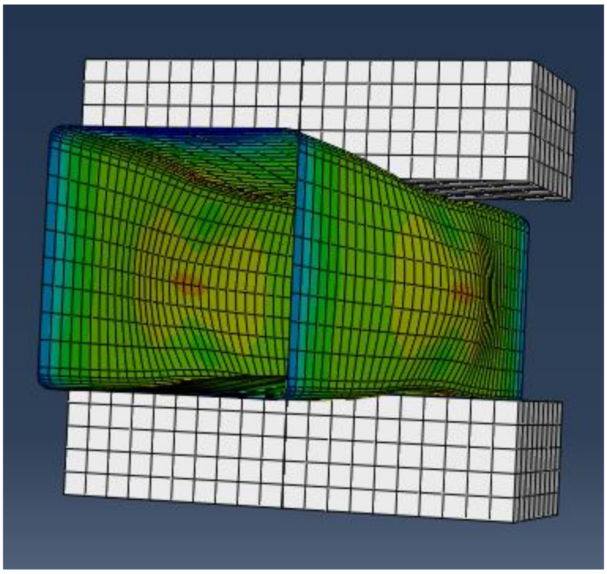

(b) Specimen in finite element analysis

**Figure 3:** Web crippling failure of Specimen ITF100×100×3.0N90


(a) Specimen in the test

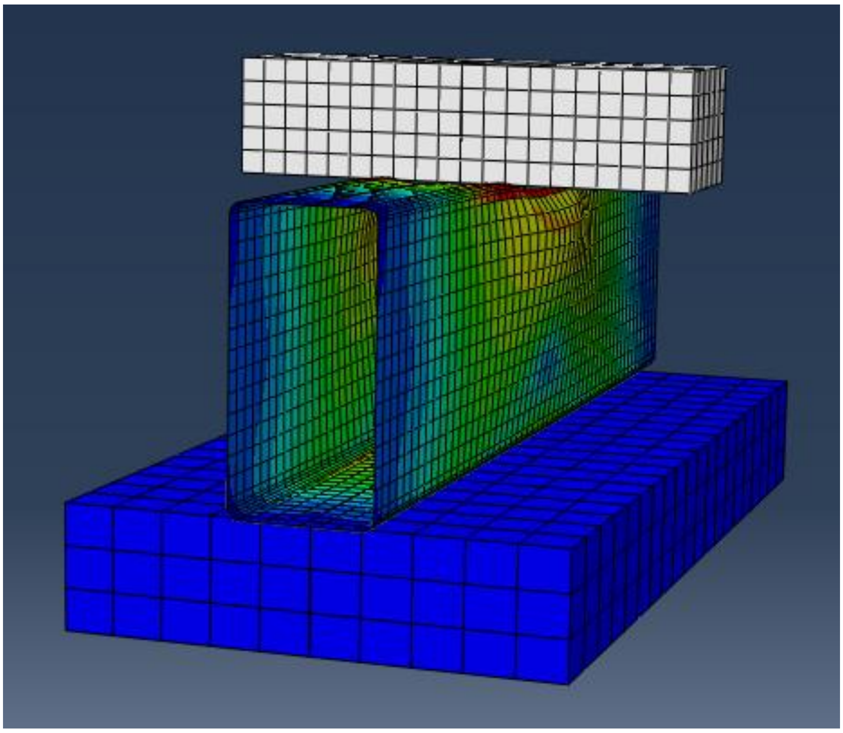

(b) Specimen in finite element analysis

**Figure 4:** Comparison of test and numerical model for Specimen IL120×60×3.0N60

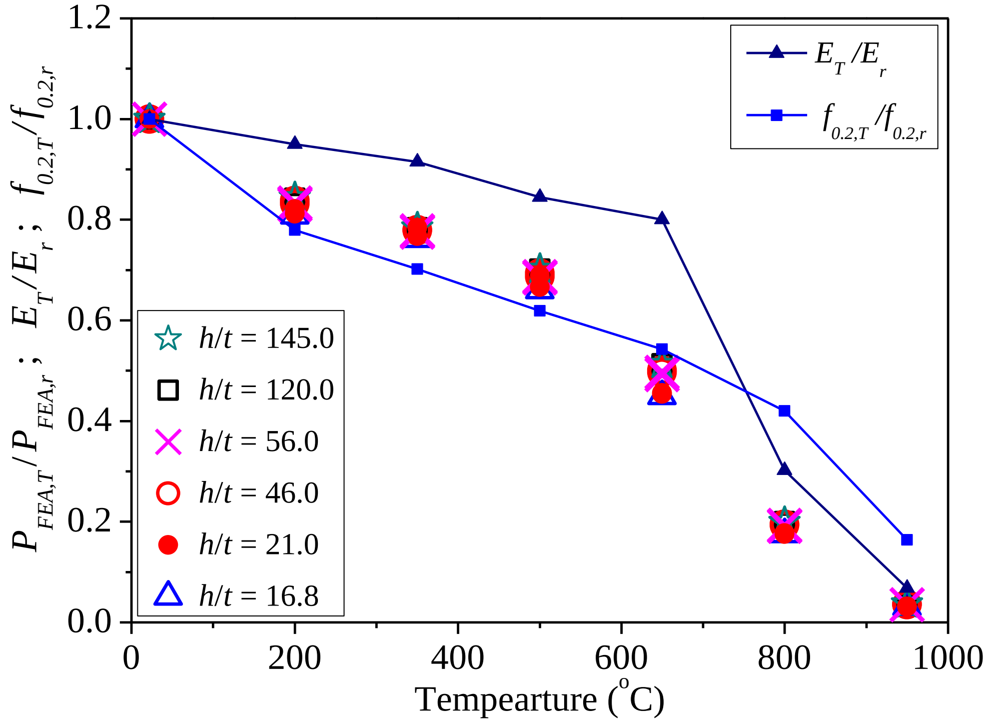


**Figure 5:** Comparison of reduction factors for IOF loading condition

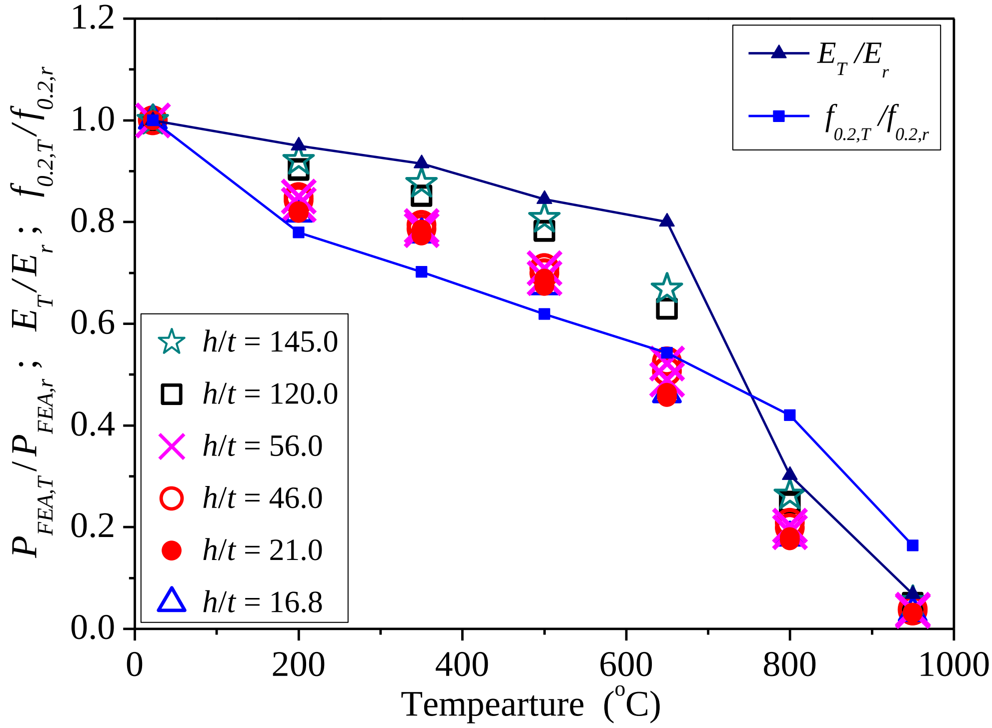


**Figure 6:** Comparison of reduction factors for ITF loading condition

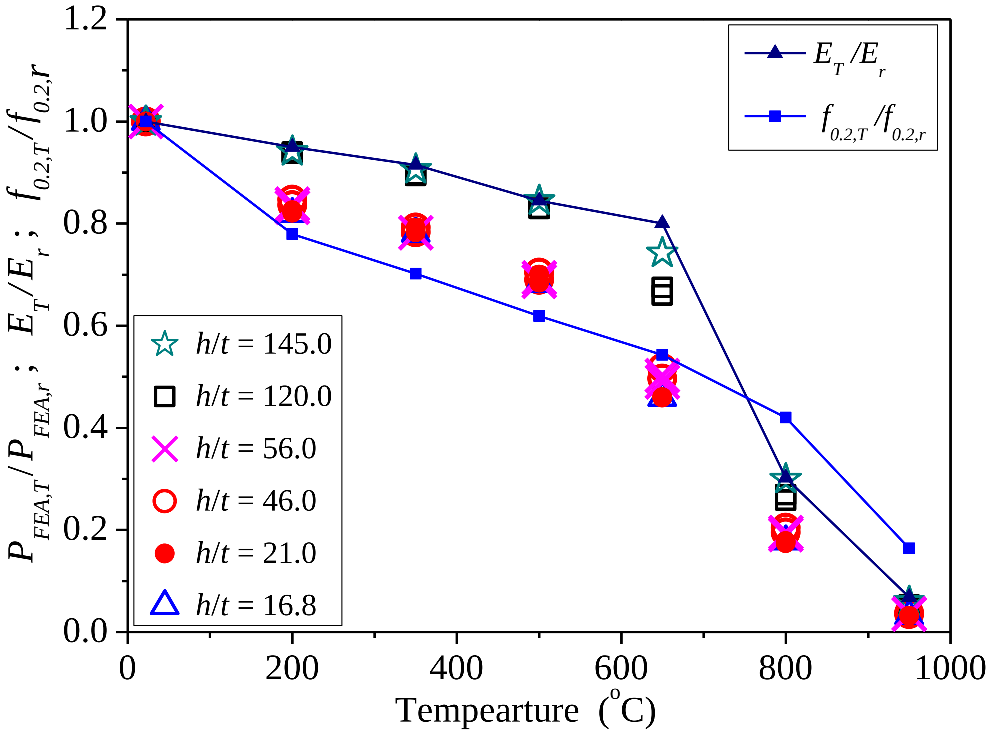


**Figure 7:** Comparison of reduction factors for IL loading condition

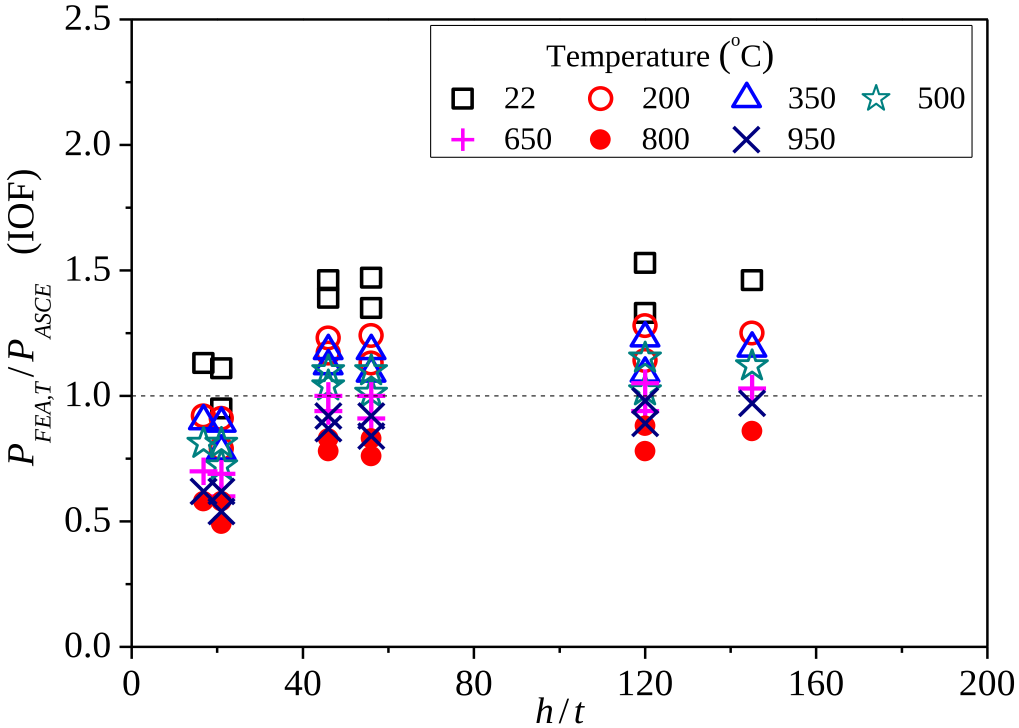


(a) ASCE [3] for IOF

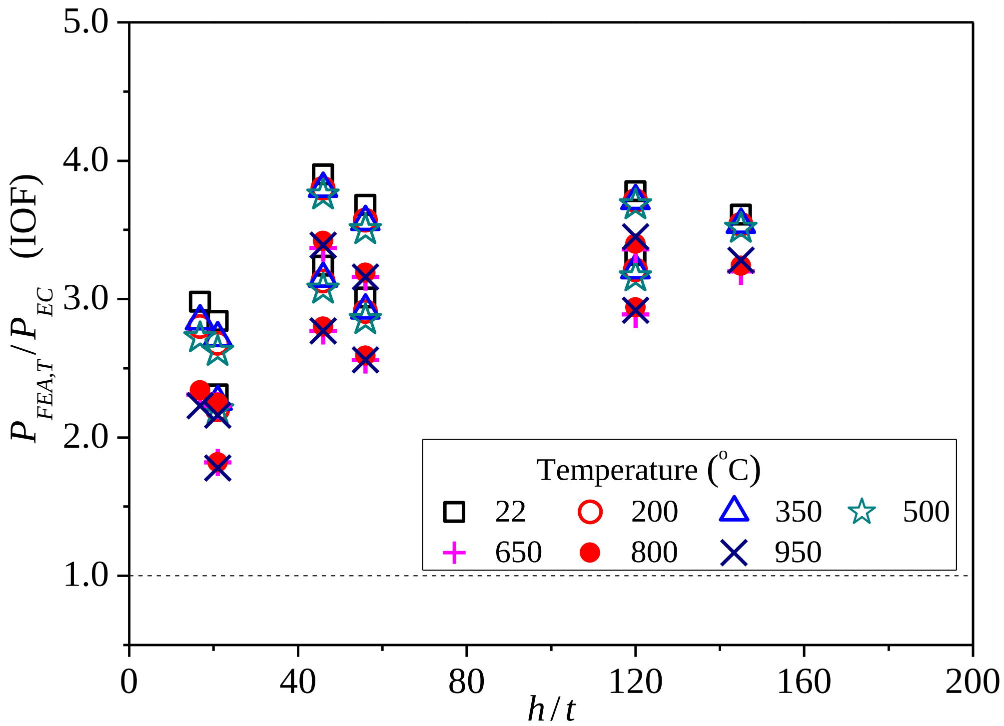


(b) EC3-1.3 [58] for IOF

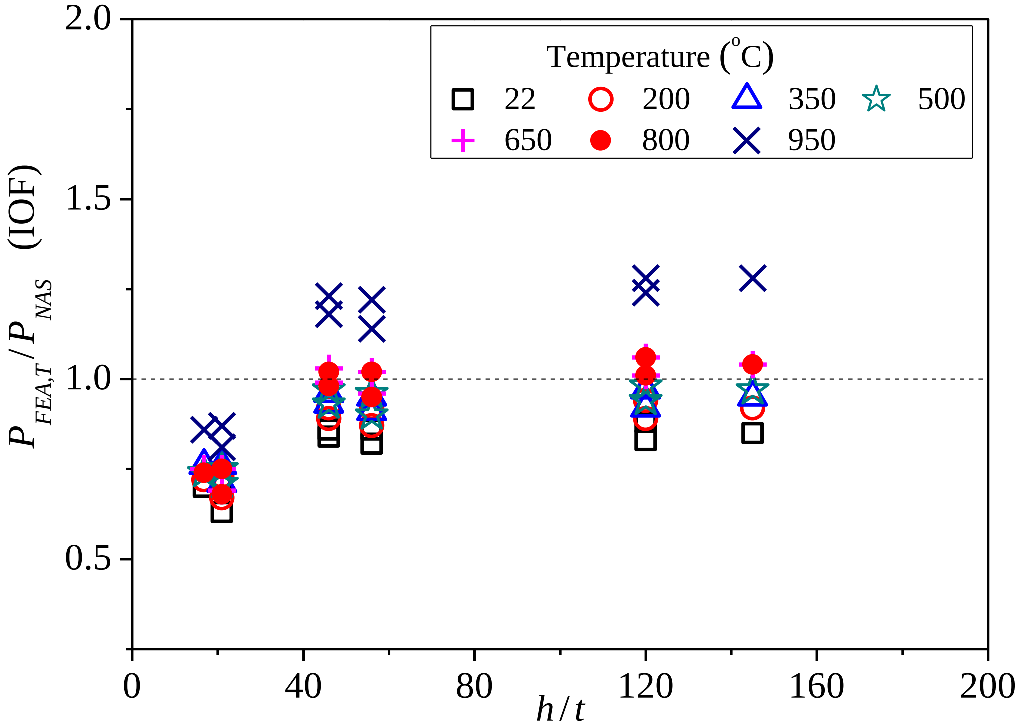


(c) NAS [39] for IOF

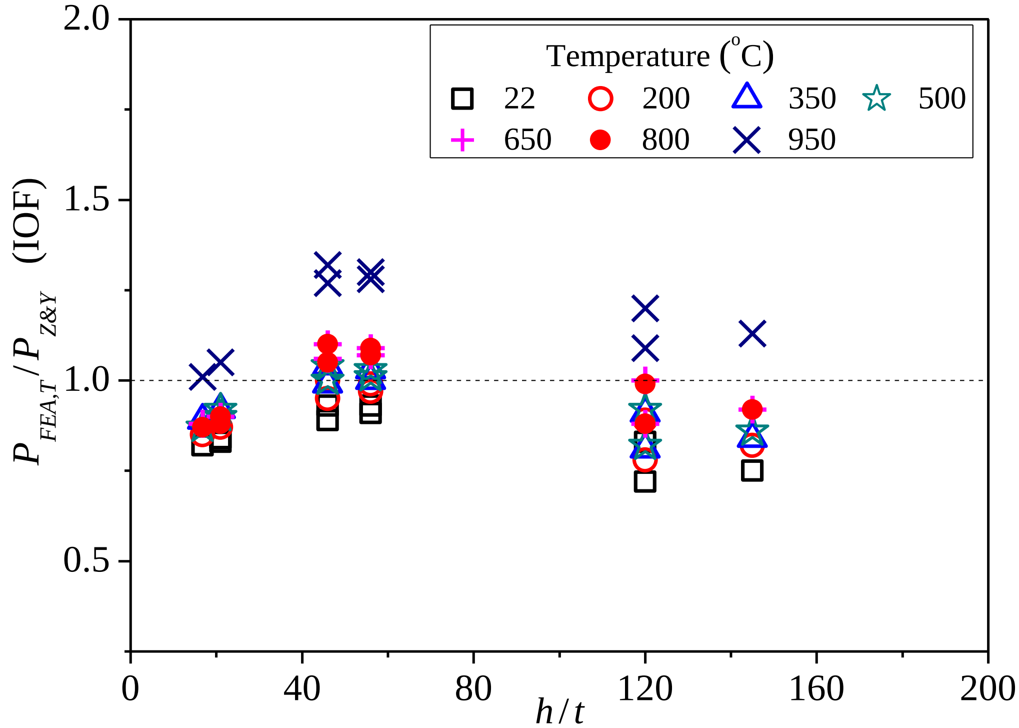


(d) Zhou and Young [30] for IOF

**Figure 8:** Comparison of FE results with predictions for IOF loading condition

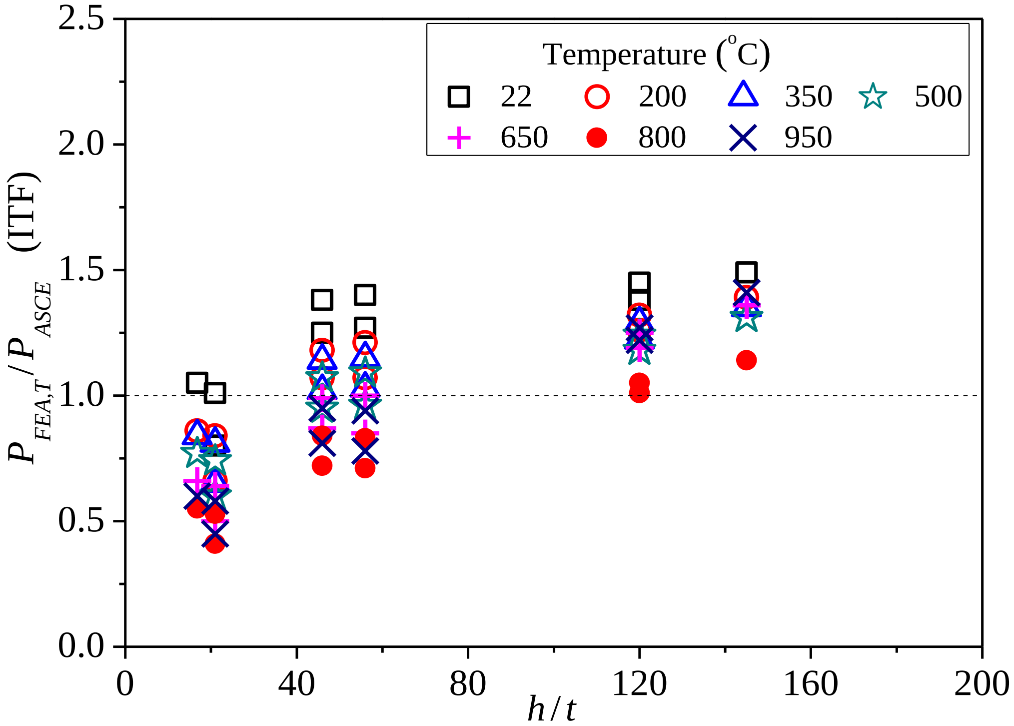


(a) ASCE [3] for ITF

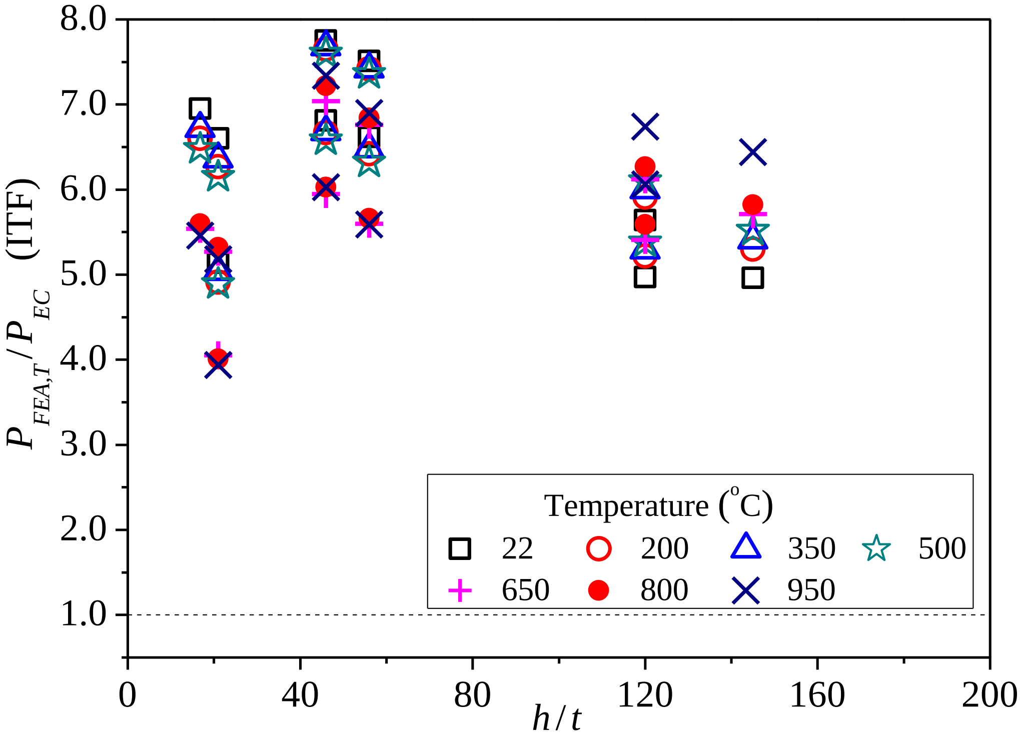


(b) EC3-1.3 [58] for ITF

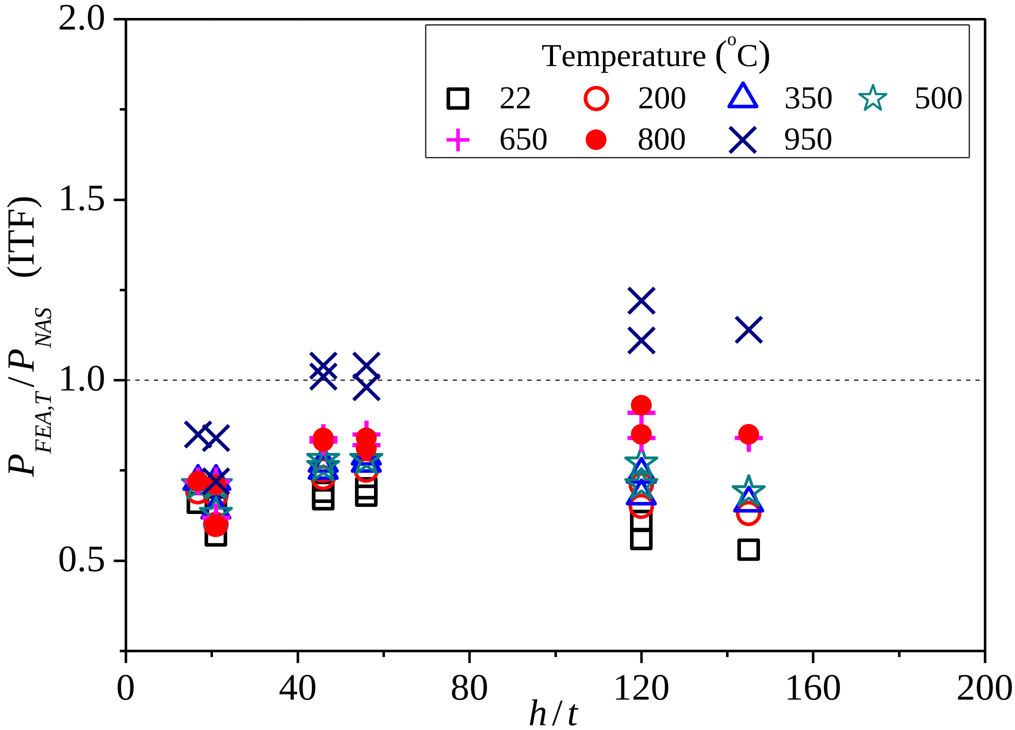


(c) NAS [39] for ITF

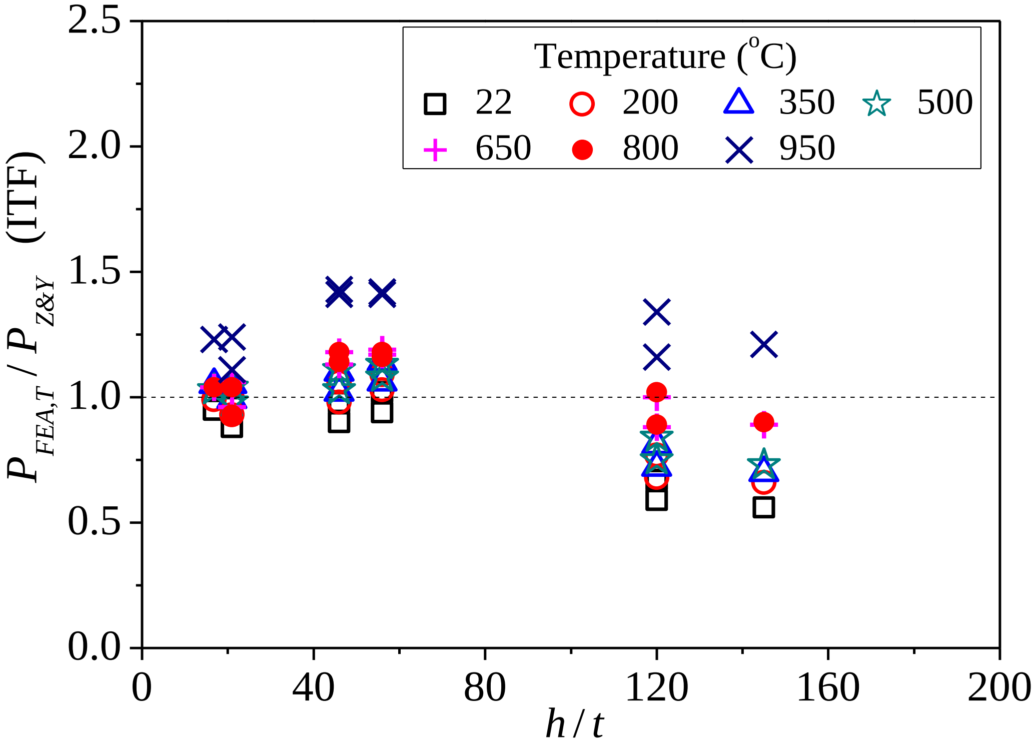


(d) Zhou and Young [30] for ITF

**Figure 9:** Comparison of FE results with predictions for ITF loading condition

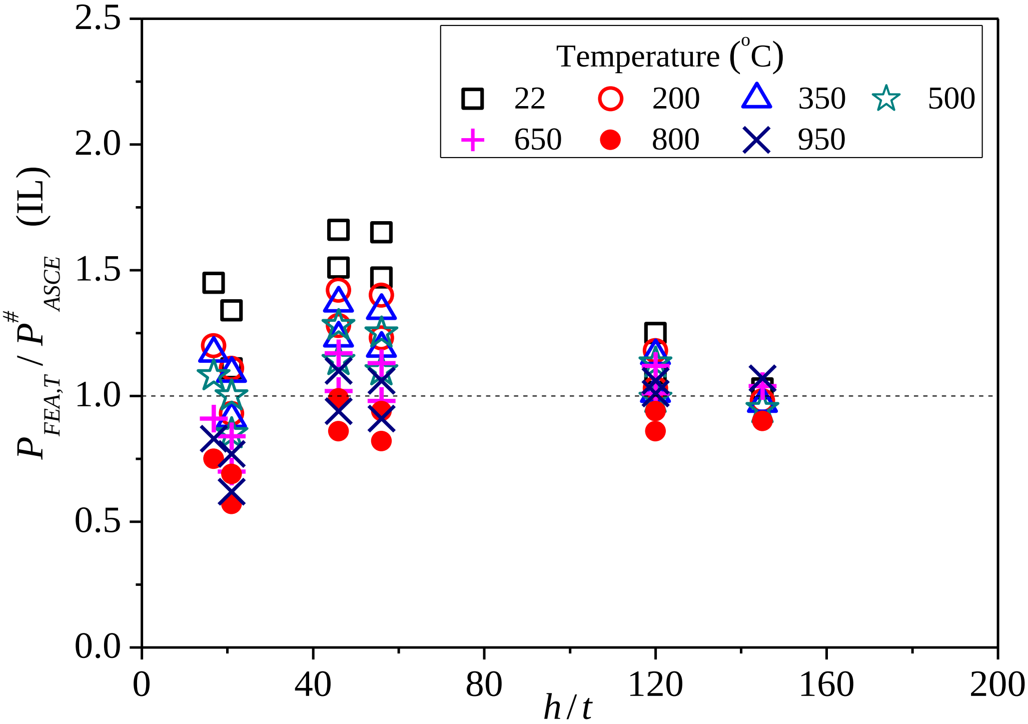


(a) Using ASCE IOF design rule [3] for IL

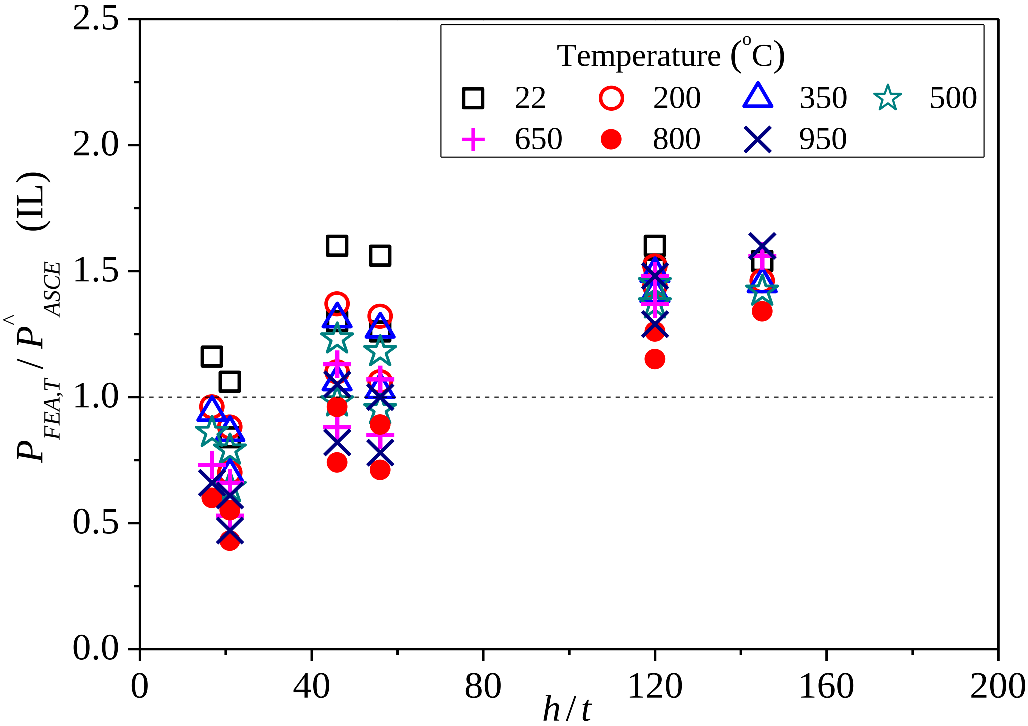


(b) Using ASCE ITF design rule [3] for IL

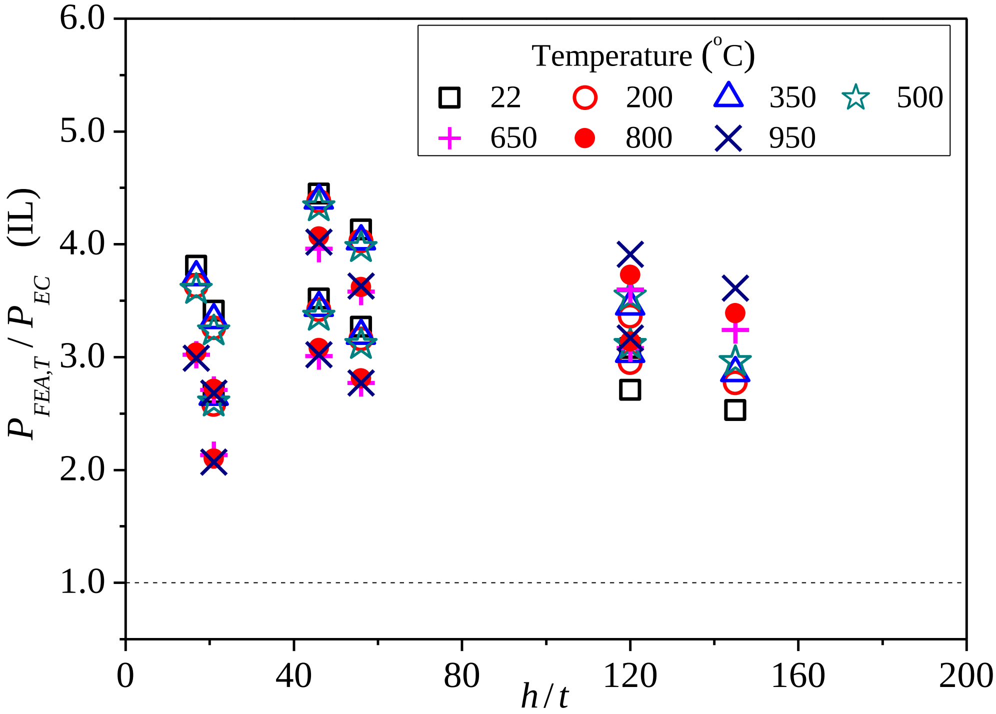


(c) Using EC3-1.3 [58] for IL

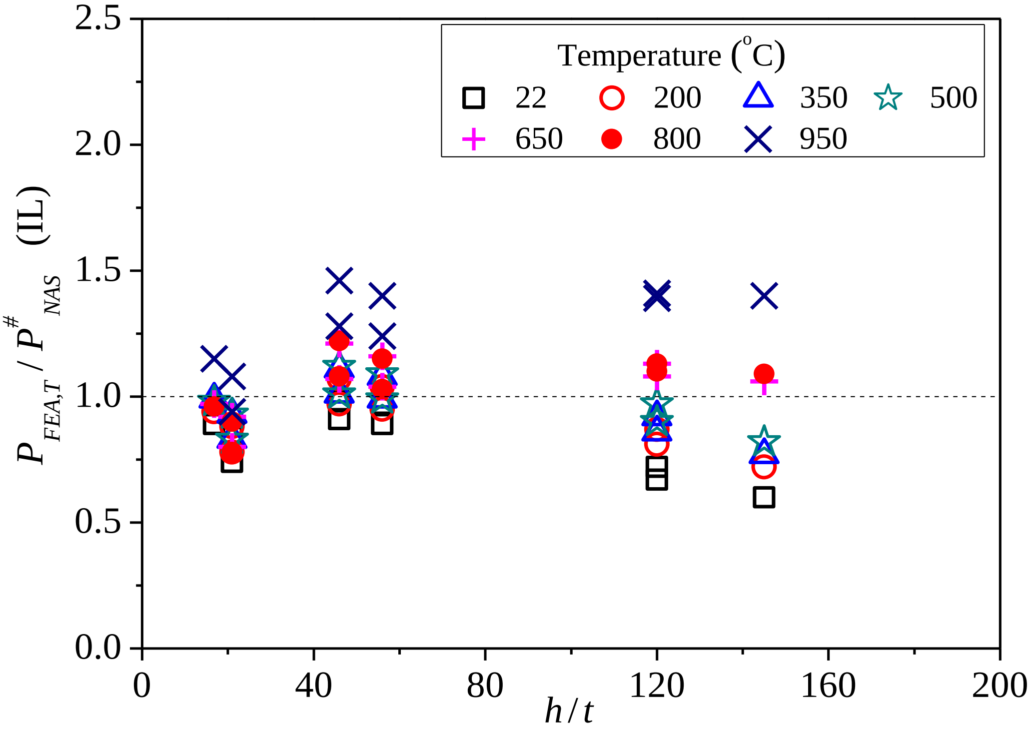


(d) Using NAS IOF design rule [39] for IL

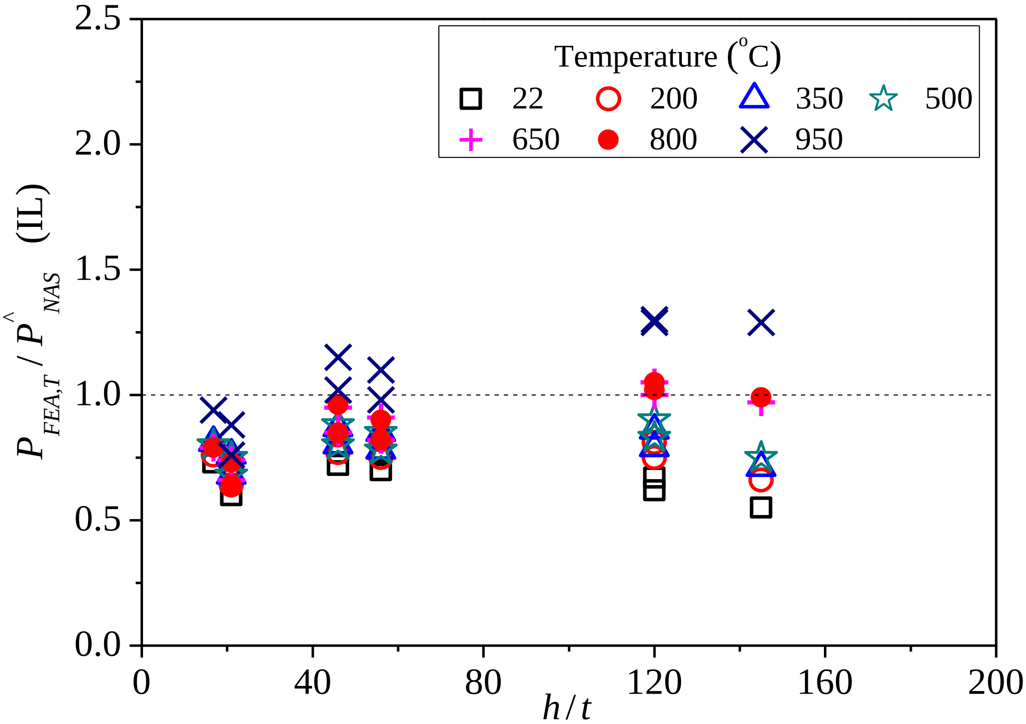


(e) Using NAS ITF design rule [39] for IL

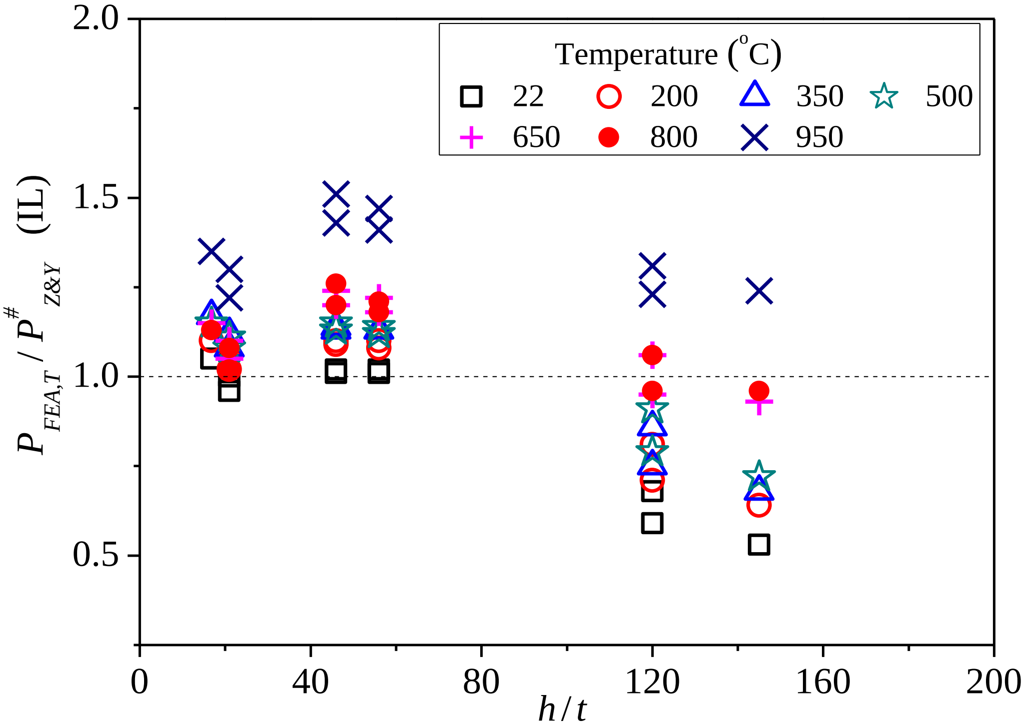


(f) Using Zhou and Young IOF coefficients [30] for IL

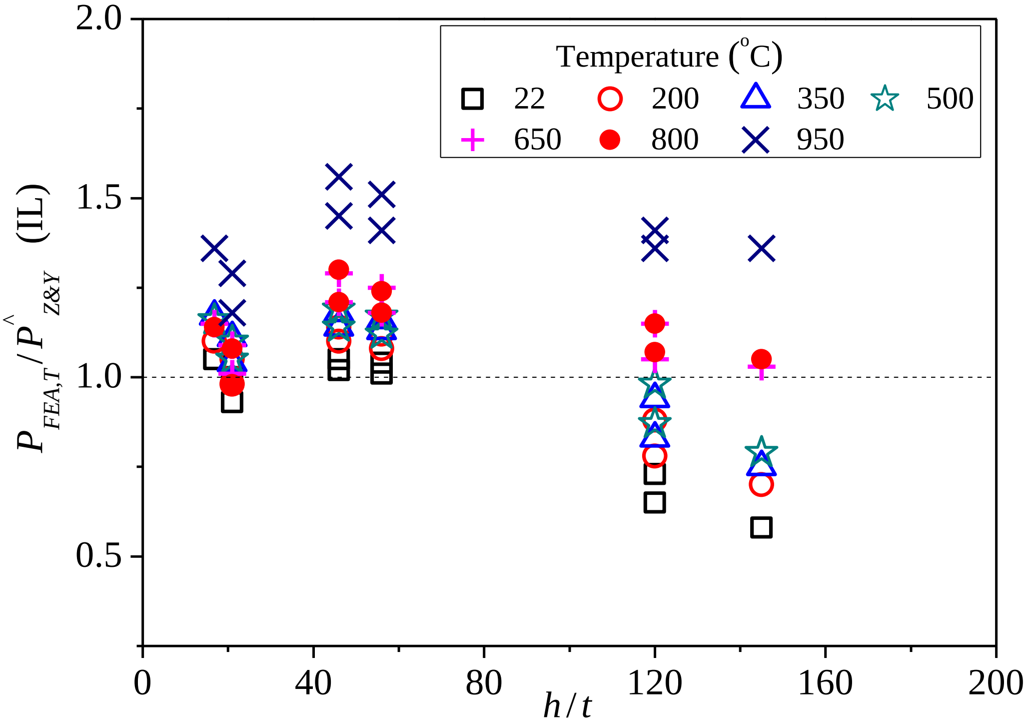


(g) Using Zhou and Young ITF coefficients [30] for IL

**Figure 10:** Comparison of FE results with predictions for IL loading condition

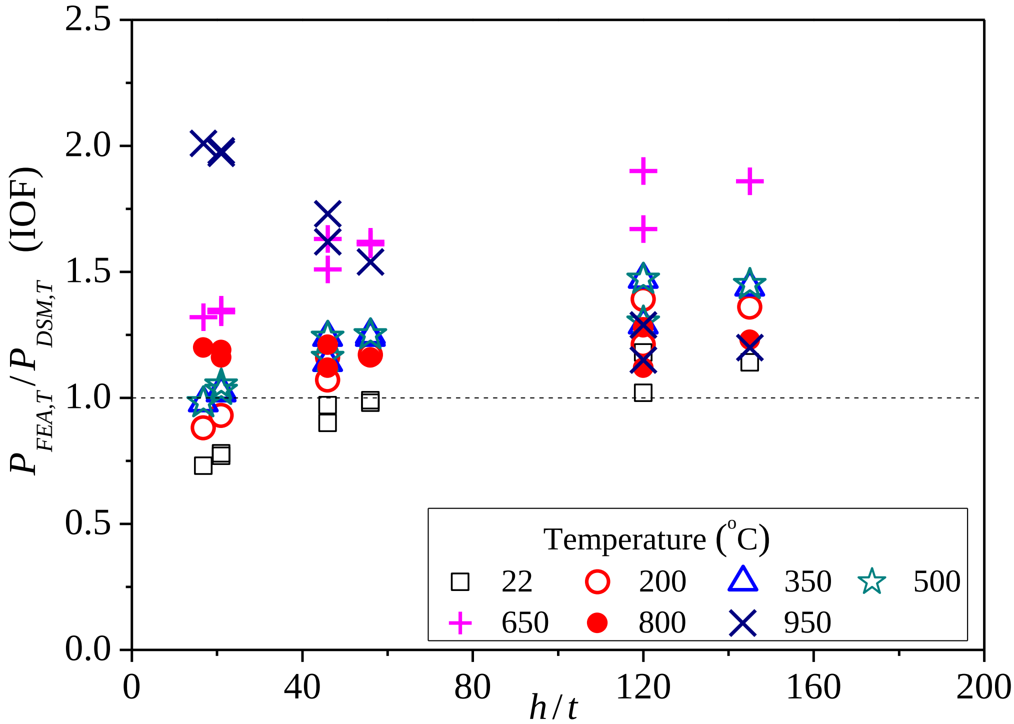


(a) Proposed predictions for IOF loading condition

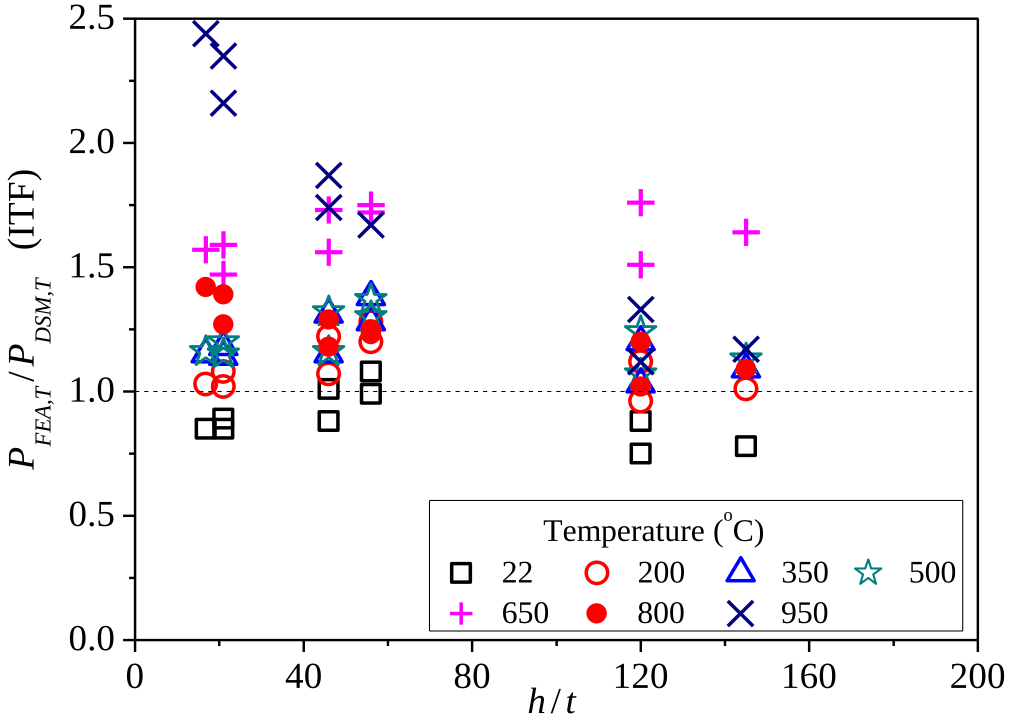


(b) Proposed predictions for ITF loading condition

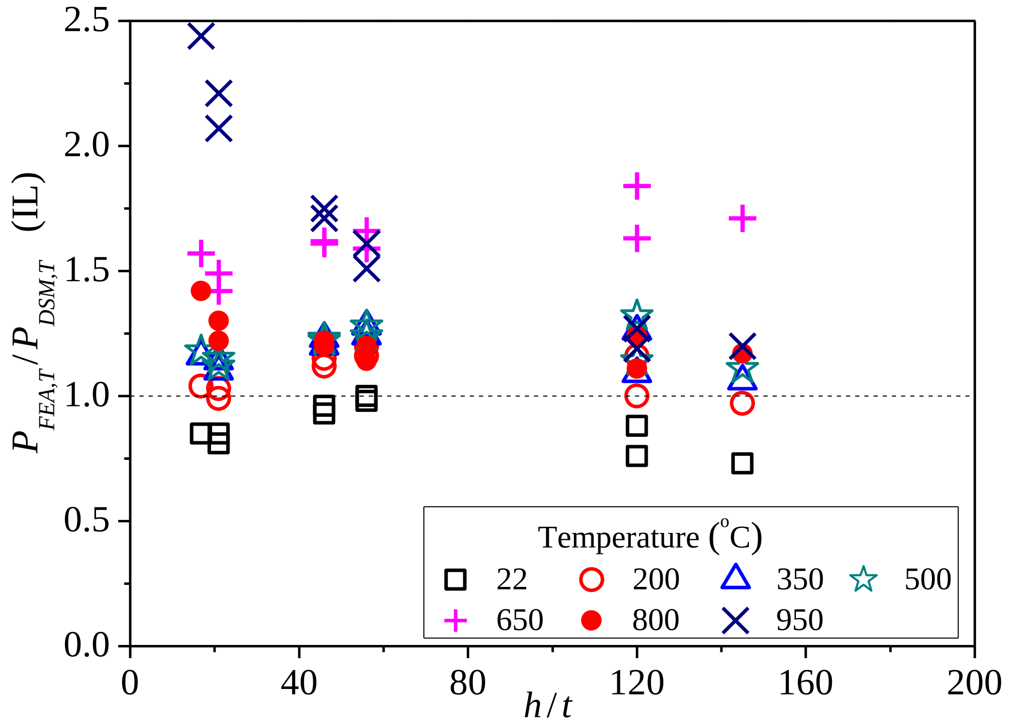


(c) Proposed predictions for IL loading condition

**Figure 11:** Comparison of FE results with proposed predictions at elevated temperatures

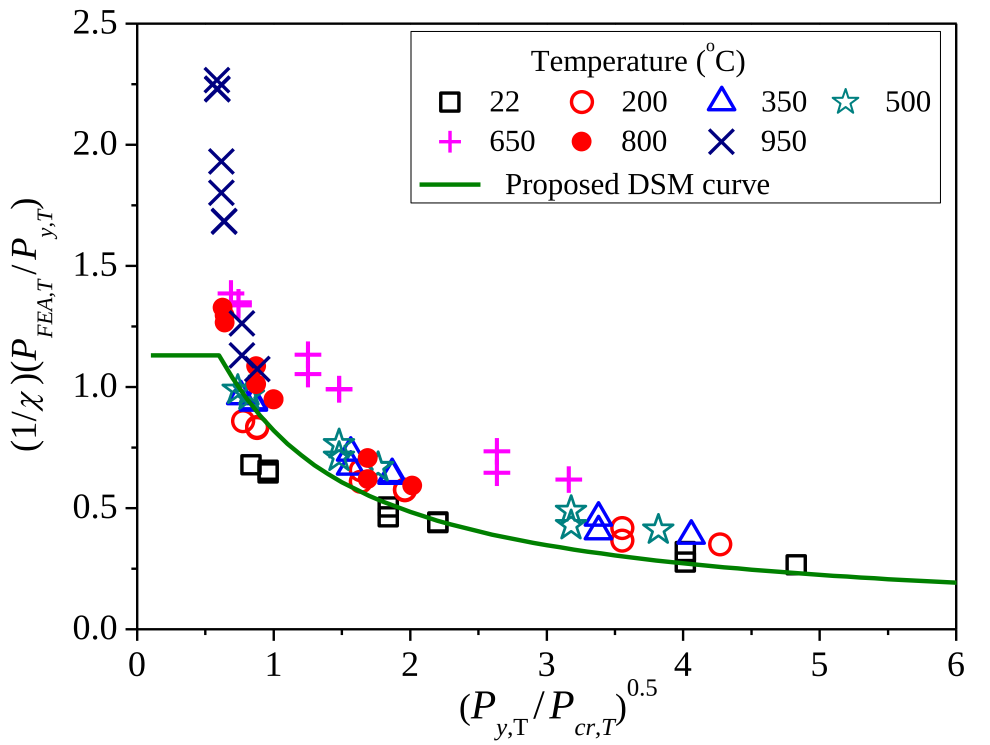


**Figure 12:** Comparison of FE results with modified DSM curve for IOF loading condition

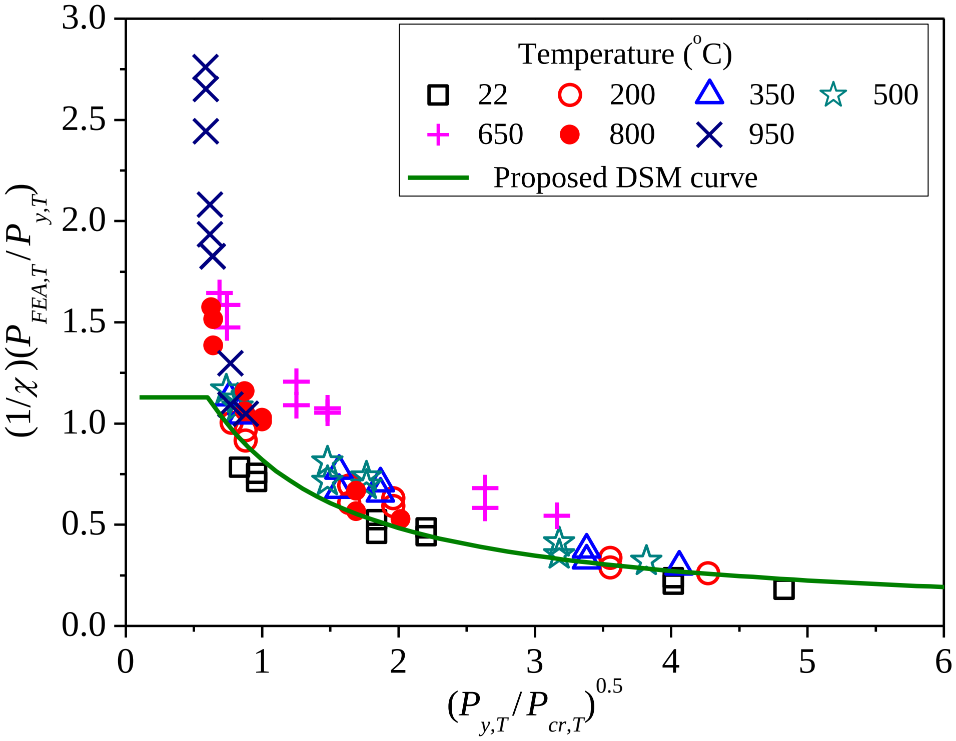


**Figure 13:** Comparison of FE results with modified DSM curve for ITF loading condition

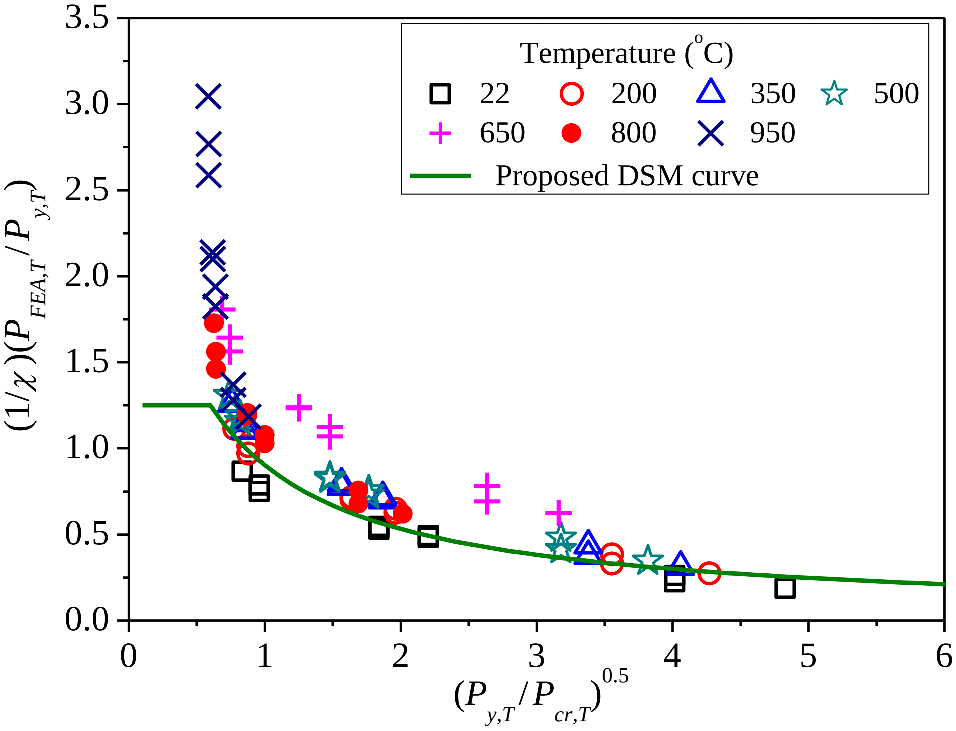


**Figure 14:** Comparison of FE results with modified DSM curve for IL loading condition

**Table 1:** Material properties of CFLDSS at room temperatures [37]

| Stainless steel grade | Section $H \times B \times t$ (mm) | $E_r$ GPa | $f_{0.2,r}$ MPa | $f_{u,r}$ MPa |
|---|---|---|---|---|
| EN 1.4162 | 50×20×1.5 | 194 | 656 | 777 |
| EN 1.4062 | 40×60×2.0 | 199 | 600 | 756 |
| | 60×40×2.0 | 199 | 600 | 756 |
| | 60×120×3.0 | 206 | 620 | 736 |
| | 80×150×3.0 | 194 | 491 | 722 |
| | 100×100×3.0 | 202 | 557 | 701 |
| | 120×60×3.0 | 206 | 620 | 736 |
| | 150×80×3.0 | 194 | 491 | 722 |

**Table 2:** Comparison of test strengths with FE predictions for IOF loading condition

| Specimen labelling | $P_t$ (kN) | $P_{FEA,r}$ (kN) | $P_t/P_{FEA,r}$ |
|---|---|---|---|
| IOF40×60×2.0N30 | 31.4 | 27.4 | 1.15 |
| IOF40×60×2.0N60 | 32.2 | 30.9 | 1.04 |
| IOF50×20×1.5N30 | 21.1 | 18.0 | 1.17 |
| IOF50×20×1.5N30-r | 20.9 | 19.4 | 1.08 |
| IOF60×40×2.0N30 | 29.3 | 28.2 | 1.04 |
| IOF60×120×3.0N60 | 73.5 | 70.2 | 1.05 |
| IOF60×120×3.0N90 | 77.5 | 74.5 | 1.04 |
| IOF80×150×3.0N60 | 57.7 | 52.0 | 1.11 |
| IOF80×150×3.0N150 | 70.6 | 63.2 | 1.12 |
| IOF100×100×3.0N30 | 70.7 | 55.7 | 1.27 |
| IOF100×100×3.0N90 | 89.1 | 76.0 | 1.17 |
| IOF100×100×3.0N90-r | 89.5 | 76.5 | 1.17 |
| IOF120×60×3.0N30 | 61.1 | 56.2 | 1.09 |
| IOF120×60×3.0N60 | 71.6 | 71.1 | 1.01 |
| IOF150×80×3.0N30 | 48.4 | 46.3 | 1.05 |
| IOF150×80×3.0N90 | 62.1 | 54.9 | 1.13 |
| | | Mean | 1.10 |
| | | COV | 0.063 |

**Table 3:** Comparison of test strengths with FE predictions for ITF loading condition

| Specimen labelling | $P_t$ (kN) | $P_{FEA,r}$ (kN) | $P_t/P_{FEA,r}$ |
|---|---|---|---|
| ITF40×60×2.0N30 | 31.4 | 28.0 | 1.12 |
| ITF40×60×2.0N60 | 39.8 | 37.7 | 1.06 |
| ITF50×20×1.5N30 | 21.5 | 21.6 | 1.00 |
| ITF50×20×1.5N30-r | 21.4 | 21.6 | 0.99 |
| ITF60×40×2.0N30 | 31.7 | 29.4 | 1.08 |
| ITF60×40×2.0N30-r | 31.7 | 30.7 | 1.03 |
| ITF60×120×3.0N60 | 77.8 | 73.0 | 1.07 |
| ITF60×120×3.0N90 | 92.0 | 87.8 | 1.05 |
| ITF60×120×3.0N90-r | 91.0 | 89.4 | 1.02 |
| ITF80×150×3.0N60 | 57.3 | 48.6 | 1.18 |
| ITF80×150×3.0N150 | 78.5 | 73.1 | 1.07 |
| ITF80×150×3.0N150-r | 78.9 | 72.3 | 1.09 |
| ITF100×100×3.0N30 | 72.4 | 61.3 | 1.18 |
| ITF100×100×3.0N90 | 85.9 | 81.6 | 1.05 |
| ITF120×60×3.0N30 | 73.4 | 65.8 | 1.12 |
| ITF120×60×3.0N60 | 78.9 | 81.3 | 0.97 |
| ITF150×80×3.0N30 | 54.8 | 45.1 | 1.22 |
| ITF150×80×3.0N90 | 69.6 | 64.4 | 1.08 |
| | | | 1.08 |
| | | | 0.063 |

**Table 4:** Comparison of test strengths with FE predictions for IL loading condition

| Specimen labelling | $P_t$ (kN) | $P_{FEA,r}$ (kN) | $P_t/P_{FEA,r}$ |
|---|---|---|---|
| IL40×60×2.0N30 | 35.9 | 34.2 | 1.05 |
| IL40×60×2.0N60 | 48.4 | 45.5 | 1.06 |
| IL40×60×2.0N60-r | 48.4 | 47.5 | 1.02 |
| IL50×20×1.5N30 | 22.2 | 23.3 | 0.95 |
| IL50×20×1.5N30-r | 22.3 | 23.9 | 0.93 |
| IL60×40×2.0N30 | 34.0 | 34.5 | 0.99 |
| IL60×40×2.0N50 | 40.2 | 41.3 | 0.97 |
| IL60×40×2.0N50-r | 39.8 | 40.3 | 0.99 |
| IL60×120×3.0N60 | 86.6 | 80.5 | 1.08 |
| IL60×120×3.0N120 | 128.8 | 119.3 | 1.08 |
| IL80×150×3.0N60 | 65.2 | 58.6 | 1.11 |
| IL80×150×3.0N150 | 89.3 | 92.7 | 0.96 |
| IL80×150×3.0N150-r | 88.7 | 84.3 | 1.05 |
| IL100×100×3.0N30 | 74.3 | 61.9 | 1.20 |
| IL100×100×3.0N90 | 102.0 | 83.8 | 1.22 |
| IL120×60×3.0N30 | 73.4 | 65.3 | 1.12 |
| IL120×60×3.0N60 | 81.5 | 79.3 | 1.03 |
| IL150×80×3.0N30 | 55.7 | 52.1 | 1.07 |
| IL150×80×3.0N90 | 70.3 | 63.7 | 1.10 |
| | | Mean | 1.05 |
| | | COV | 0.075 |

**Table 5:** Summary of the ratios of test strength-to-FE prediction

| Loading condition | Number | | $P_t/P_{FEA}$ |
|---|---|---|---|
| IOF, ITF and IL | 53 | Mean | 1.08 |
| | | COV | 0.069 |

**Table 6:** Design of CFLDSS (EN 1.4162) specimens for parametric study at elevated temperatures

| Loading condition | Section ($H$×$B$×$t$) | | | Bearing length | Parameters | | |
|---|---|---|---|---|---|---|---|
| | $H$ (mm) | $B$ (mm) | $t$ (mm) | $N$ (mm) | $r/t$ | $N/t$ | $h/t$ |
| IOF, ITF and IL | 250 | 250 | 2.0 | 250 | 1.5 | 125.0 | 120.0 |
| | 250 | 250 | 2.0 | 125 | 1.5 | 62.5 | 120.0 |
| | 250 | 250 | 5.0 | 250 | 1.0 | 50.0 | 46.0 |
| | 250 | 250 | 5.0 | 125 | 1.0 | 25.0 | 46.0 |
| | 250 | 250 | 12.0 | 250 | 1.0 | 20.8 | 16.8 |
| | 300 | 200 | 2.0 | 200 | 1.5 | 100.0 | 145.0 |
| | 300 | 200 | 5.0 | 200 | 1.0 | 40.0 | 56.0 |
| | 300 | 200 | 5.0 | 100 | 1.0 | 20.0 | 56.0 |
| | 300 | 200 | 12.0 | 200 | 1.0 | 16.7 | 21.0 |
| | 300 | 200 | 12.0 | 100 | 1.0 | 8.3 | 21.0 |

**Table 7:** Material properties of CFLDSS at elevated temperatures [26]

| | Nominal Temperature (°C) | | | | | | |
|---|---|---|---|---|---|---|---|
| | 22# | 200 | 350 | 500 | 650 | 800 | 950 |
| $E_T$ (GPa) | 200 | 190 | 183 | 169 | 160 | 60.4 | 13.5 |
| $f_{0.2,T}$ (MPa) | 724 | 564 | 508 | 448 | 393 | 304 | 119 |
| $f_{u,T}$ (MPa) | 862 | 710 | 696 | 627 | 514 | 358 | 138 |

Note: "#" represents room (ambient) temperature.

**Table 8:** Web crippling strength of CFLDSS specimens at elevated temperatures

| Specimen labelling | FEA load per web at different temperature levels (kN) | | | | | | |
|---|---|---|---|---|---|---|---|
| | 22[#] °C | 200 °C | 350 °C | 500 °C | 650 °C | 800 °C | 950 °C |
| IOF250×250×2.0N125 | 44.7 | 37.2 | 34.6 | 30.8 | 22.6 | 8.8 | 1.6 |
| IOF250×250×2.0N250 | 51.0 | 43.0 | 40.0 | 35.8 | 26.2 | 10.2 | 1.9 |
| IOF250×250×5.0N125 | 240.1 | 199.6 | 186.9 | 164.7 | 119.1 | 46.3 | 8.4 |
| IOF250×250×5.0N250 | 289.0 | 242.1 | 225.4 | 200.7 | 144.8 | 56.4 | 10.3 |
| IOF250×250×12.0N250 | 1143.0 | 923.5 | 871.5 | 754.0 | 514.6 | 200.0 | 35.0 |
| IOF300×200×2.0N200 | 48.7 | 41.1 | 38.2 | 34.2 | 25.0 | 9.7 | 1.8 |
| IOF300×200×5.0N100 | 223.2 | 185.2 | 173.6 | 152.6 | 109.9 | 42.7 | 7.8 |
| IOF300×200×5.0N200 | 272.8 | 227.3 | 211.3 | 187.5 | 135.6 | 52.7 | 9.6 |
| IOF300×200×12.0N100 | 885.7 | 727.5 | 694.7 | 610.3 | 404.2 | 155.4 | 28.0 |
| IOF300×200×12.0N200 | 1090.8 | 885.5 | 837.1 | 726.7 | 494.9 | 192.7 | 33.9 |
| ITF250×250×2.0N125 | 33.2 | 30.0 | 28.3 | 26.0 | 20.9 | 8.3 | 1.7 |
| ITF250×250×2.0N250 | 37.7 | 34.0 | 32.1 | 29.5 | 23.7 | 9.3 | 1.8 |
| ITF250×250×5.0N125 | 250.1 | 210.7 | 196.7 | 174.8 | 126.6 | 49.4 | 9.1 |
| ITF250×250×5.0N250 | 284.6 | 241.6 | 225.9 | 201.8 | 149.8 | 59.1 | 11.0 |
| ITF250×250×12.0N250 | 1320.7 | 1079.0 | 1024.4 | 890.6 | 610.6 | 237.3 | 42.6 |
| ITF300×200×2.0N200 | 33.1 | 30.5 | 29.0 | 26.7 | 22.1 | 8.7 | 1.8 |
| ITF300×200×5.0N100 | 243.2 | 202.9 | 190.7 | 167.9 | 119.2 | 46.3 | 8.4 |
| ITF300×200×5.0N200 | 275.9 | 234.5 | 218.5 | 195.6 | 144.0 | 56.0 | 10.4 |
| ITF300×200×12.0N100 | 978.1 | 802.7 | 767.5 | 672.9 | 445.9 | 170.0 | 30.7 |
| ITF300×200×12.0N200 | 1254.1 | 1025.6 | 969.7 | 845.1 | 581.3 | 225.3 | 40.4 |
| IL250×250×2.0N125 | 36.5 | 34.3 | 32.7 | 30.3 | 24.1 | 9.4 | 1.8 |
| IL250×250×2.0N250 | 41.6 | 39.0 | 37.2 | 34.5 | 28.1 | 11.2 | 2.2 |
| IL250×250×5.0N125 | 260.8 | 217.9 | 204.3 | 180.0 | 129.4 | 50.8 | 9.2 |
| IL250×250×5.0N250 | 329.5 | 279.1 | 260.8 | 232.0 | 170.3 | 67.2 | 12.2 |
| IL250×250×12.0N250 | 1461.6 | 1197.5 | 1141.4 | 997.4 | 671.2 | 260.1 | 47.0 |
| IL300×200×2.0N200 | 34.1 | 32.1 | 30.9 | 28.8 | 25.3 | 10.2 | 2.0 |
| IL300×200×5.0N100 | 242.3 | 201.5 | 189.4 | 166.4 | 118.8 | 46.3 | 8.4 |
| IL300×200×5.0N200 | 306.4 | 256.9 | 239.6 | 212.5 | 153.7 | 59.8 | 11.0 |
| IL300×200×12.0N100 | 1029.6 | 850.4 | 814.1 | 720.6 | 472.6 | 179.2 | 32.5 |
| IL300×200×12.0N200 | 1308.8 | 1074.7 | 1025.0 | 895.7 | 602.3 | 232.4 | 42.2 |

**Table 9:** Coefficients for the web crippling design by the unified design equation

| Resources | Loading condition | Coefficients | | | | | Limits ($\theta$ = 90°) | | | |
|---|---|---|---|---|---|---|---|---|---|---|
| | | $C$ | $C_R$ | $C_N$ | $C_h$ | $\phi$ | $r/t$ | $N/t$ | $h/t$ | $N/h$ |
| NAS [39] | IOF | 13.0 | 0.23 | 0.14 | 0.01 | 0.90 | ≤ 5.0 | ≤ 210 | ≤ 200 | ≤ 2.0 |
| | ITF | 24.0 | 0.52 | 0.15 | 0.001 | 0.80 | ≤ 3.0 | ≤ 210 | ≤ 200 | ≤ 2.0 |
| Zhou and Young [30] | IOF | 6.0 | 0.17 | 0.37 | 0.02 | 0.70 | ≤ 5.5 | ≤ 100 | ≤ 87 | ≤ 1.6 |
| | ITF | 8.2 | 0.27 | 0.27 | 0.001 | 0.70 | ≤ 5.5 | ≤ 100 | ≤ 87 | ≤ 1.6 |

Note: The table is suitable to stiffened or partially stiffened flanges that unfastened to support.

**Table 10:** Comparison of test strengths with predicted strengths for IOF loading condition

| Temp. (°C) | | $P_{FEA,T}/P_{ASCE}$ | $P_{FEA,T}/P_{EC}$ | $P_{FEA,T}/P_{NAS}$ | $P_{FEA,T}/P_{Z\&Y}$ | $P_{FEA,T}/P_{DSM,T}$ |
|---|---|---|---|---|---|---|
| 22# | Mean | 1.32 | 3.27 | 0.80 | 0.84 | 0.95 |
| | COV | 0.144 | 0.152 | 0.109 | 0.085 | 0.163 |
| 200 | Mean | 1.11 | 3.15 | 0.85 | 0.90 | 1.13 |
| | COV | 0.154 | 0.162 | 0.120 | 0.084 | 0.155 |
| 350 | Mean | 1.07 | 3.17 | 0.88 | 0.94 | 1.21 |
| | COV | 0.146 | 0.155 | 0.112 | 0.083 | 0.139 |
| 500 | Mean | 0.99 | 3.10 | 0.88 | 0.94 | 1.22 |
| | COV | 0.154 | 0.164 | 0.121 | 0.082 | 0.137 |
| 650 | Mean | 0.89 | 2.77 | 0.93 | 0.98 | 1.58 |
| | COV | 0.184 | 0.191 | 0.153 | 0.095 | 0.129 |
| 800 | Mean | 0.74 | 2.80 | 0.92 | 0.97 | 1.18 |
| | COV | 0.186 | 0.193 | 0.155 | 0.096 | 0.041 |
| 950 | Mean | 0.82 | 2.77 | 1.11 | 1.17 | 1.60 |
| | COV | 0.199 | 0.207 | 0.169 | 0.102 | 0.200 |
| All conditions | Mean | 0.99 | 3.00 | 0.91 | 0.96 | 1.27 |
| | COV | 0.243 | 0.179 | 0.169 | 0.132 | 0.228 |
| | Resistance factor, $\phi$ | 0.70 | 0.91 | 0.90 | 0.70 | 0.80 |
| | Reliability index, $\beta$ | 2.50 | 5.56 | 1.79 | 3.04 | 2.92 |

Note: "#" represents room (ambient) temperature.

**Table 11:** Comparison of test strengths with predicted strengths for ITF loading condition

| Temp. (°C) | | $P_{FEA,T}/P_{ASCE}$ | $P_{FEA,T}/P_{EC}$ | $P_{FEA,T}/P_{NAS}$ | $P_{FEA,T}/P_{Z\&Y}$ | $P_{FEA,T}/P_{DSM,T}$ |
|---|---|---|---|---|---|---|
| 22# | Mean | 1.25 | 6.30 | 0.63 | 0.84 | 0.90 |
| | COV | 0.181 | 0.165 | 0.095 | 0.201 | 0.116 |
| 200 | Mean | 1.09 | 6.24 | 0.69 | 0.92 | 1.10 |
| | COV | 0.215 | 0.147 | 0.076 | 0.170 | 0.096 |
| 350 | Mean | 1.05 | 6.31 | 0.73 | 0.96 | 1.19 |
| | COV | 0.214 | 0.140 | 0.069 | 0.166 | 0.088 |
| 500 | Mean | 0.99 | 6.24 | 0.73 | 0.97 | 1.21 |
| | COV | 0.233 | 0.135 | 0.068 | 0.151 | 0.079 |
| 650 | Mean | 0.93 | 5.74 | 0.80 | 1.05 | 1.63 |
| | COV | 0.303 | 0.144 | 0.108 | 0.110 | 0.064 |
| 800 | Mean | 0.78 | 5.84 | 0.80 | 1.05 | 1.24 |
| | COV | 0.311 | 0.150 | 0.117 | 0.110 | 0.099 |
| 950 | Mean | 0.90 | 5.97 | 0.99 | 1.30 | 1.75 |
| | COV | 0.356 | 0.165 | 0.153 | 0.093 | 0.266 |
| All conditions | Mean | 1.00 | 6.09 | 0.77 | 1.01 | 1.29 |
| | COV | 0.280 | 0.148 | 0.176 | 0.188 | 0.263 |
| | $\phi$ | 0.70 | 0.91 | 0.80 | 0.70 | 0.80 |
| | $\beta$ | 2.33 | 8.43 | 1.59 | 2.89 | 2.75 |

Note: "#" represents room (ambient) temperature.

**Table 12:** Comparison of test strengths with predicted strengths for IL loading condition

| Temp. (ºC) | | $P_{FEA,T}/P_{ASCE}^{\#}$ | $P_{FEA,T}/P_{ASCE}^{\wedge}$ | $P_{FEA,T}/P_{EC}$ | $P_{FEA,T}/P_{NAS}^{\#}$ | $P_{FEA,T}/P_{NAS}^{\wedge}$ | $P_{FEA,T}/P_{Z\&Y}^{\#}$ | $P_{FEA,T}/P_{Z\&Y}^{\wedge}$ | $P_{FEA,T}/P_{DSM,T}$ |
|---|---|---|---|---|---|---|---|---|---|
| 22# | Mean | 1.35 | 1.34 | 3.36 | 0.82 | 0.68 | 0.89 | 0.91 | 0.87 |
| | COV | 0.170 | 0.196 | 0.190 | 0.160 | 0.105 | 0.229 | 0.200 | 0.107 |
| 200 | Mean | 1.18 | 1.18 | 3.35 | 0.90 | 0.75 | 0.97 | 0.99 | 1.08 |
| | COV | 0.142 | 0.237 | 0.164 | 0.124 | 0.087 | 0.185 | 0.155 | 0.079 |
| 350 | Mean | 1.14 | 1.15 | 3.41 | 0.95 | 0.79 | 1.02 | 1.05 | 1.18 |
| | COV | 0.132 | 0.238 | 0.155 | 0.113 | 0.079 | 0.178 | 0.147 | 0.067 |
| 500 | Mean | 1.07 | 1.09 | 3.38 | 0.96 | 0.80 | 1.03 | 1.06 | 1.20 |
| | COV | 0.125 | 0.260 | 0.149 | 0.101 | 0.083 | 0.158 | 0.128 | 0.059 |
| 650 | Mean | 0.99 | 1.03 | 3.11 | 1.04 | 0.87 | 1.11 | 1.14 | 1.61 |
| | COV | 0.147 | 0.347 | 0.169 | 0.114 | 0.141 | 0.099 | 0.082 | 0.071 |
| 800 | Mean | 0.83 | 0.86 | 3.17 | 1.04 | 0.87 | 1.11 | 1.14 | 1.22 |
| | COV | 0.156 | 0.361 | 0.179 | 0.124 | 0.154 | 0.095 | 0.085 | 0.071 |
| 950 | Mean | 0.94 | 0.98 | 3.19 | 1.28 | 1.07 | 1.35 | 1.39 | 1.70 |
| | COV | 0.166 | 0.390 | 0.191 | 0.135 | 0.175 | 0.078 | 0.078 | 0.255 |
| All conditions | Mean | 1.07 | 1.09 | 3.28 | 1.00 | 0.83 | 1.07 | 1.10 | 1.27 |
| | COV | 0.208 | 0.302 | 0.167 | 0.181 | 0.188 | 0.188 | 0.176 | 0.255 |
| | $\phi$ | 0.70 | 0.70 | 0.91 | 0.90 | 0.80 | 0.70 | 0.70 | 0.80 |
| | $\beta$ | 2.95 | 2.45 | 6.00 | 2.06 | 1.82 | 3.06 | 3.23 | 2.76 |

Note: "#" represents room (ambient) temperature.

**Table 13:** Coefficients for web crippling design of CFLDSS tubular sections at elevated temperatures

| Load condition | $a$ | $b$ | $n$ | $\lambda_k$ | $\gamma$ | $\phi$ |
|---|---|---|---|---|---|---|
| IOF | 1.00 | 0.18 | 0.45 | 0.60 | 1.13 | 0.80 |
| ITF | 1.00 | 0.18 | 0.45 | 0.60 | 1.13 | 0.80 |
| IL | 1.10 | 0.18 | 0.45 | 0.60 | 1.25 | 0.80 |

Note: The table is suitable to stiffened or partially stiffened flanges that unfastened to support; The proposed coefficients apply when $10 \le h/t \le 145$, $r_i/t \le 2.0$, $N/t \le 150$, $N/h \le 1.5$ and $\theta = 90^{\circ}$.

**Table 14:** Comparison of test strengths with predictions for IOF loading condition at room temperature

| Specimen labelling | *h/t* | *r/t* | *N/t* | *N/h* | $P_t$ and $P_{FEA,r}$ (kN) | $P_{DSM,T}$ (kN) | $P_t/P_{DSM,T}$ and $P_{FEA,r}/P_{DSM,T}$ |
|---|---|---|---|---|---|---|---|
| IOF40×60×2.0N30 | 16.3 | 0.9 | 15.0 | 0.92 | 31.4 | 27.6 | 1.14 |
| IOF40×60×2.0N60 | 16.2 | 0.9 | 29.7 | 1.83 | 32.2 | 38.4 | 0.84 |
| IOF50×20×1.5N30 | 29.9 | 0.7 | 19.9 | 0.67 | 21.1 | 21.5 | 0.98 |
| IOF50×20×1.5N30-r | 28.8 | 0.6 | 19.1 | 0.66 | 20.9 | 23.9 | 0.87 |
| IOF60×40×2.0N30 | 25.8 | 0.9 | 14.8 | 0.57 | 29.3 | 28.1 | 1.04 |
| IOF60×120×3.0N60 | 15.4 | 1.1 | 19.5 | 1.27 | 73.5 | 72.6 | 1.01 |
| IOF60×120×3.0N90 | 15.5 | 1.1 | 29.3 | 1.90 | 77.5 | 87.7 | 0.88 |
| IOF80×150×3.0N60 | 19.7 | 2.1 | 19.4 | 0.98 | 57.7 | 41.4 | 1.39 |
| IOF80×150×3.0N150 | 20.2 | 1.9 | 48.5 | 2.40 | 70.6 | 65.1 | 1.08 |
| IOF100×100×3.0N30 | 28.3 | 1.1 | 9.7 | 0.34 | 70.7 | 48.6 | 1.45 |
| IOF100×100×3.0N90 | 28.1 | 1.1 | 29.1 | 1.03 | 89.1 | 67.7 | 1.32 |
| IOF100×100×3.0N90-r | 28.2 | 1.1 | 29.0 | 1.03 | 89.5 | 68.5 | 1.31 |
| IOF120×60×3.0N30 | 34.8 | 1.2 | 9.8 | 0.28 | 61.1 | 55.1 | 1.11 |
| IOF120×60×3.0N60 | 35.0 | 1.0 | 19.5 | 0.56 | 71.6 | 67.4 | 1.06 |
| IOF150×80×3.0N30 | 42.9 | 2.1 | 9.7 | 0.23 | 48.4 | 33.3 | 1.45 |
| IOF150×80×3.0N90 | 42.7 | 2.0 | 29.1 | 0.68 | 62.1 | 43.9 | 1.42 |
| | | | | | | Mean | 1.15 |
| | | | | | | COV | 0.186 |
| | | | | | | Resistance factor, $\phi$ | 0.80 |
| | | | | | | Reliability index, $\beta$ | 2.78 |

**Table 15:** Comparison of test and FE strengths with predictions for ITF loading condition at room temperature

| Specimen labelling | $h/t$ | $r/t$ | $N/t$ | $N/h$ | $P_t$ and $P_{FEA,r}$ (kN) | $P_{DSM,T}$ (kN) | $P_t/P_{DSM,T}$ and $P_{FEA,r}/P_{DSM,T}$ |
|---|---|---|---|---|---|---|---|
| ITF20×50×1.5N30 | 9.8 | 0.5 | 19.2 | 1.95 | 25.6 | 24.5 | 1.05 |
| ITF20×50×1.5N30-r | 9.7 | 0.7 | 19.7 | 2.03 | 26.1 | 22.2 | 1.18 |
| ITF20×50×1.5N50 | 10.1 | 0.6 | 33.4 | 3.32 | 36.5 | 30.3 | 1.20 |
| ITF40×60×2.0N30 | 16.2 | 1.0 | 15.0 | 0.93 | 31.4 | 27.2 | 1.15 |
| ITF40×60×2.0N60 | 16.2 | 0.9 | 29.9 | 1.85 | 39.8 | 38.1 | 1.04 |
| ITF50×20×1.5N30 | 30.3 | 0.7 | 20.1 | 0.66 | 21.5 | 21.0 | 1.02 |
| ITF50×20×1.5N30-r | 30.3 | 0.7 | 20.1 | 0.66 | 21.4 | 21.0 | 1.02 |
| ITF60×40×2.0N30 | 25.7 | 1.1 | 14.9 | 0.58 | 31.7 | 27.0 | 1.17 |
| ITF60×40×2.0N30-r | 25.8 | 0.9 | 14.8 | 0.57 | 31.7 | 28.1 | 1.13 |
| ITF60×120×3.0N60 | 16.1 | 0.9 | 19.7 | 1.22 | 77.8 | 74.2 | 1.05 |
| ITF60×120×3.0N90 | 15.4 | 1.1 | 29.2 | 1.90 | 92.0 | 88.2 | 1.04 |
| ITF60×120×3.0N90-r | 15.4 | 1.0 | 29.1 | 1.89 | 91.0 | 89.6 | 1.02 |
| ITF80×150×3.0N60 | 19.9 | 2.1 | 19.4 | 0.97 | 57.3 | 41.4 | 1.38 |
| ITF80×150×3.0N150 | 20.1 | 2.0 | 48.6 | 2.42 | 78.5 | 63.8 | 1.23 |
| ITF80×150×3.0N150-r | 19.7 | 2.1 | 48.6 | 2.47 | 78.9 | 63.3 | 1.25 |
| ITF100×100×3.0N30 | 28.5 | 1.1 | 9.8 | 0.34 | 72.4 | 48.1 | 1.51 |
| ITF100×100×3.0N90 | 28.3 | 1.1 | 29.1 | 1.03 | 85.9 | 68.8 | 1.25 |
| ITF120×60×3.0N30 | 34.9 | 1.1 | 9.7 | 0.28 | 73.4 | 57.1 | 1.29 |
| ITF120×60×3.0N60 | 35.2 | 0.9 | 19.5 | 0.56 | 78.9 | 68.9 | 1.14 |
| ITF150×80×3.0N30 | 43.3 | 2.0 | 9.7 | 0.22 | 54.8 | 33.6 | 1.63 |
| ITF150×80×3.0N90 | 43.0 | 2.1 | 29.1 | 0.68 | 69.6 | 43.1 | 1.62 |
| | | | | | | Mean | 1.21 |
| | | | | | | COV | 0.155 |
| | | | | | | Resistance factor, $\phi$ | 0.80 |
| | | | | | | Reliability index, $\beta$ | 3.18 |

**Table 16:** Comparison of test and FE strengths with predictions for IL loading condition at room temperature

| Specimen labelling | $h/t$ | $r/t$ | $N/t$ | $N/h$ | $P_t$ and $P_{FEA,r}$ (kN) | $P_{DSM,T}$ (kN) | $P_t/P_{DSM,T}$ and $P_{FEA,r}/P_{DSM,T}$ |
|---|---|---|---|---|---|---|---|
| IL20×50×1.5N30 | 9.9 | 0.7 | 19.8 | 1.99 | 29.9 | 24.8 | 1.20 |
| IL20×50×1.5N50 | 10.1 | 0.6 | 33.1 | 3.26 | 41.1 | 34.1 | 1.20 |
| IL40×60×2.0N30 | 16.3 | 0.8 | 14.8 | 0.91 | 35.9 | 32.2 | 1.11 |
| IL40×60×2.0N60 | 16.5 | 0.8 | 29.9 | 1.81 | 48.4 | 43.3 | 1.12 |
| IL40×60×2.0N60-r | 16.3 | 0.7 | 29.4 | 1.81 | 48.4 | 45.3 | 1.07 |
| IL50×20×1.5N30 | 29.3 | 0.7 | 19.5 | 0.67 | 22.2 | 24.6 | 0.90 |
| IL50×20×1.5N30-r | 29.8 | 0.5 | 19.7 | 0.66 | 22.3 | 25.1 | 0.89 |
| IL60×40×2.0N30 | 25.9 | 0.7 | 14.6 | 0.56 | 34.0 | 33.2 | 1.03 |
| IL60×40×2.0N50 | 26.1 | 0.8 | 24.6 | 0.94 | 40.2 | 38.2 | 1.05 |
| IL60×40×2.0N50-r | 26.5 | 0.8 | 25.0 | 0.94 | 39.8 | 37.1 | 1.07 |
| IL60×120×3.0N60 | 15.6 | 1.1 | 19.6 | 1.26 | 86.6 | 78.9 | 1.10 |
| IL60×120×3.0N120 | 15.8 | 0.9 | 39.2 | 2.48 | 128.8 | 116.5 | 1.11 |
| IL80×150×3.0N60 | 19.9 | 2.0 | 19.4 | 0.97 | 65.2 | 46.1 | 1.41 |
| IL80×150×3.0N150 | 21.2 | 1.5 | 48.8 | 2.30 | 89.3 | 77.6 | 1.15 |
| IL80×150×3.0N150-r | 20.5 | 1.9 | 48.7 | 2.38 | 88.7 | 72.1 | 1.23 |
| IL100×100×3.0N30 | 28.3 | 1.2 | 9.7 | 0.34 | 74.3 | 52.4 | 1.42 |
| IL100×100×3.0N90 | 27.8 | 1.4 | 29.2 | 1.05 | 102.0 | 69.8 | 1.46 |
| IL120×60×3.0N30 | 34.8 | 1.0 | 9.7 | 0.28 | 73.4 | 63.8 | 1.15 |
| IL120×60×3.0N60 | 35.3 | 1.0 | 19.6 | 0.56 | 81.5 | 74.5 | 1.09 |
| IL150×80×3.0N30 | 42.9 | 2.1 | 9.7 | 0.23 | 55.7 | 36.6 | 1.52 |
| IL150×80×3.0N90 | 42.9 | 2.0 | 29.1 | 0.68 | 70.3 | 48.0 | 1.46 |
| | | | | | | Mean | 1.18 |
| | | | | | | COV | 0.153 |
| | | | | | | Resistance factor, $\phi$ | 0.80 |
| | | | | | | Reliability index, $\beta$ | 3.12 |